Journal of Materials Research and Technology 44 (2026) 2615–2636

Contents lists available at ScienceDirect

Journal of Materials Research and Technology

journal homepage: www.elsevier.com/locate/jmrt

Artificial intelligence and statistical analysis -driven prediction and optimization of tensile properties in biomass/resin epoxy composites

Maroua Moudjari [a], Ramy M. Hafez [b], Omar Ahmed Alhelali [c], Nabil Talbi [d,*], Mohamed Kezzar [d], Farhan Lafta Rashid [e], Mohamed Rafik Sari [f], Aya M. Al-Zuheiri [g], Yazen M. Alawaideh [h], Ioan-Lucian Popa [i,j,**], Ibrahim Mahariq [k,l,m,n,o,***]

[a] Technogical Department, Higher Normal School of Technological Education of Skikda, Azzaba, Skikda, 21000, Algeria
[b] Department of Mathematics and Statistics, College of Science, Imam Mohammad Ibn Saud Islamic University (IMSIU), Riyadh, 11432, Saudi Arabia
[c] Department of Mathematics, Applied College at Mahail, Aseer, King Khalid University, Abha, Saudi Arabia
[d] Materials and Energy Engineering Laboratory (LMGE), Technology Department, Faculty of Technology, 20 Aout 1955 University of Skikda, PO Box 26, 21000, Skikda, Algeria
[e] Petroleum Engineering Department, College of Engineering, University of Kerbala, Karbala, 56001, Iraq
[f] Mechanics of Materials and Plant Maintenance Research Laboratory (LR3MI), Mechanical Engineering Department, Faculty of Engineering, Badji Mokhtar University of Annaba (UBMA), PO Box 12, 23052, Annaba, Algeria
[g] Department of Basic Sciences, Middle East University, Amman, 11831, Jordan
[h] Department of Computer Engineering, Biruni University, 34010, Istanbul, Turkey
[i] Department of Computing, Mathematics and Electronics, "1 Decembrie 1918" University of Alba Iulia, 15, 510009, Alba Iulia, Romania
[j] Faculty of Mathematics and Computer Science, Transilvania University of Brasov, Iluiu Maniu Streat 50, 5000917, Romania
[k] College of Engineering and Architecture, Gulf University for Science and Technology, Mishref, Kuwait
[l] Department of Electrical and Electronic Engineering, Faculty of Engineering and Architecture, Istanbul Gelisim University, Avcılar- Istanbul, 34310, Istanbul, Türkiye
[m] Najjad Zeenni Faculty of Engineering, Al-Quds University, Jerusalem, Palestine
[n] Department of Medical Research, China Medical University Hospital, China Medical University, Taichung, Taiwan
[o] University College, Korea University, Seoul, 02481, South Korea

ARTICLE INFO

Keywords:
Biomass composites
Epoxy resin
Tensile properties
Artificial neural networks
Response surface methodology
ANOVA

ABSTRACT

This study explores the tensile behavior of epoxy composites reinforced with agricultural waste—walnut, almond, and pistachio shell particles—at weight fractions of 10%, 15%, and 25%. Composites were fabricated via hand lay-up, and mechanical properties were evaluated according to ASTM D3039 standards. Scanning Electron Microscopy (SEM) analysis revealed uniform particle dispersion and strong matrix-filler adhesion in walnut composites, while almond and pistachio composites exhibited particle agglomeration and microvoids at higher loadings. Tensile testing showed that walnut-filled composites achieved the highest strength (105.12 MPa) and ductility (strain ~4.9%), whereas almond and pistachio fillers reached peak strength at intermediate loadings but suffered reduced elongation due to interfacial defects. Artificial Neural Networks (ANNs) accurately predicted tensile stress, strain, and young's modulus, with regression coefficients close to 0.99, while Response Surface Methodology (RSM) identified the optimal combination of filler type, weight fraction, and cross-sectional area for maximizing tensile performance. These results demonstrate that both filler selection and loading critically influence composite properties, and that AI-driven modeling provides a reliable tool for predicting and optimizing the mechanical behavior of biomass-reinforced epoxy composites.

* Corresponding author.
** Corresponding author. Department of Computing, Mathematics and Electronics, "1 Decembrie 1918" University of Alba Iulia, 15, 510009, Alba Iulia, Romania.
*** Corresponding author. College of Engineering and Architecture, Gulf University for Science and Technology, Mishref, Kuwait.
E-mail addresses: marouamoudjari@gmail.com (M. Moudjari), rHafez@imamu.edu.sa (R.M. Hafez), omaralhelali535@gmail.com (O.A. Alhelali), nabil_talbi@yahoo.fr (N. Talbi), Kezzar_m@yahoo.com (M. Kezzar), farhan.lefta@uokerbala.edu.iq (F.L. Rashid), sari_rafik10@yahoo.fr (M. Rafik Sari), alzuheiri@meu.edu.jo (A.M. Al-Zuheiri), yazen_awaida@yahoo.com (Y.M. Alawaideh), lucian.papo@aub.ro (I.-L. Popa), ibmahariq@gmail.com (I. Mahariq).

https://doi.org/10.1016/j.jmrt.2026.07.281
Received 30 March 2026; Received in revised form 28 June 2026; Accepted 29 July 2026
Available online 1 August 2026

Abbreviations

ANN	Artificial Neural Network
RSM	Response Surface Methodology
SEM	Scanning Electron Microscopy
MPa	Megapascal
wt%	Weight Percent
ASTM	American Society for Testing and Materials
DOEs	Design of Experiments
LY556	Epoxy Resin Grade LY556
HY951	Epoxy Hardener HY951
MSE	Mean Squared Error
Wb	Walnut Biomass
Ab	Almond Biomass
Pb	Pistachio Biomass

1. Introduction

Many researchers have been studying the use of natural fibers as load-bearing components in composite materials during the past few years [1]. A multi-phase system made of reinforcing and matrix materials is called a composite material [2]. The matrix provides strength and stiffness for structural loads by defining the composite material's volume, combining the reinforcing agent, and evenly distributing the applied load to reinforcements [3].

Powder-reinforced polymers with a thermoset or thermoplastic matrix are called polymer matrix composites (PMCs). Because of their high strength-to-weight ratio, ease of fabrication, and affordability, polymer matrix composites (PMCs) are frequently utilized in a range of industries, including automobiles, ships, and structural applications [4,5]. Synthetic fibers like glass, carbon, boron, and graphite, or natural fibers like sisal, hemp, flax, bamboo, coir, and jute can be used to strengthen polymeric composites. Because of their low density, environmental advantages, and affordability [6], natural fiber composites are appropriate for construction [7], packing [8,9], automobile interiors [10,11], and storage equipment.

Powder biomass content, length, organization, and matrix bonding all directly affect a bio composite's properties. Because the various particles employed in composites are independent, their properties have varied effects. Additionally, the demand for natural composites has grown in recent years due to weight reduction and easy access to reinforcement. An alternate material for the interiors of cars, ships, airplanes, and spacecraft is reinforced composite. Numerous researchers have documented the mechanical characteristics of natural fiber reinforced polymer composites and identified the qualities that are suitable for use in industrial settings [12].

The tensile and flexural properties of epoxy composites reinforced with coconut shell ash were studied by Rahul et al. [13]. It was intriguing to note that, when compared to clean epoxy and coconut shell ash heated to 600 °C, the coconut shell ash cooked to 800 °C produced the maximum tensile and flexural strength at 20% filler. According to Olumuyiwa et al. [14], after 120 h of testing, coconut shell particles with a 25% weight percentage demonstrated superior resistance to water absorption. However, it was found that polyethylene composites with a 25% fraction had the lowest tensile strength.

Agricultural residues, such as walnut, almond, and pistachio shells, are produced in large quantities globally and often disposed of as waste, leading to environmental pollution. Utilizing these residues as reinforcement in polymer composites not only provides a sustainable solution for waste management but also reduces the dependence on petroleum-based materials. Recent studies have demonstrated that the type of biomass filler, its particle size, chemical treatment, and weight fraction significantly affect the tensile, flexural, and impact properties of biocomposites. For instance, uniform particle dispersion and strong matrix-filler adhesion enhance load transfer and ductility, whereas filler agglomeration and interfacial voids can act as stress concentrators, reducing mechanical performance.

Despite the growing interest in biomass-reinforced epoxy composites, traditional trial-and-error approaches to optimize filler type and content are time-consuming, resource-intensive, and often insufficient for predicting performance across multiple variables. To address this limitation, Artificial Intelligence (AI) techniques, particularly ANNs, and statistical methods like Response RSM have gained attention as efficient tools for predicting and optimizing composite properties [15].

ANNs are capable of modeling complex, nonlinear relationships between input parameters (such as filler type, weight fraction, and cross-sectional area) and output responses (tensile strength, strain, and young's modulus) [16]. Similarly, RSM provides a structured statistical framework to analyze the effects of multiple factors and their interactions on a response variable, enabling identification of optimal process conditions with minimal experimental effort [17].

The integration of AI-driven predictive modeling and statistical optimization facilitates tailored design of sustainable epoxy composites with targeted mechanical properties [18]. For example, by training an ANN on experimental data, researchers can accurately predict tensile performance for a range of filler types and weight fractions without performing exhaustive physical tests [19]. RSM can then be employed to optimize these parameters to achieve maximum tensile strength or ductility [20]. This combination of computational modeling and experimental validation offers a robust, efficient approach for developing high-performance, eco-friendly composites, suitable for structural and engineering applications where both mechanical performance and sustainability are required.

Furthermore, morphological characterization techniques, such as SEM, play a pivotal role in understanding the microstructural mechanisms governing composite behavior. SEM analysis provides insights into particle dispersion, interfacial bonding, and the presence of microvoids, which directly correlate with tensile performance. By linking SEM observations with AI and statistical predictions, it is possible to establish a comprehensive understanding of the structure-property relationships in biomass/epoxy composites, paving the way for rational design strategies.

In this study, we focus on the tensile behavior of epoxy composites reinforced with walnut, almond, and pistachio shell particles at various weight fractions (10%, 15%, and 25%). Composites were fabricated using the hand lay-up method, and their mechanical performance was evaluated according to ASTM standards. SEM was employed to investigate particle dispersion and interfacial adhesion [21]. Subsequently, ANN models were developed to predict tensile stress, strain, and young's modulus, while RSM was utilized to optimize the combination of filler type, weight fraction, and cross-sectional area for maximum performance. This research demonstrates the synergistic application of AI and statistical methods in designing sustainable composites and provides a guideline for utilizing agricultural waste to produce high-performance, environmentally friendly materials.

Overall, this work aims to contribute to the growing body of knowledge on biomass-reinforced epoxy composites by integrating experimental characterization, AI-based predictive modeling, and statistical optimization. The outcomes highlight the potential of agricultural waste fillers in achieving mechanically robust and sustainable polymer composites, and emphasize the importance of computational tools in accelerating material development while minimizing experimental effort. By addressing the interplay between filler characteristics, mechanical performance, and AI-driven optimization, this study provides a framework for the rational design of next-generation eco-friendly composites suitable for industrial applications, it's also particularly relevant since it also addresses the valorization of agricultural waste as reinforcement in polymer matrix composites who will help better position the mechanical performance of the composites developed in the present work relative to other bio-based hybrid systems [22].

In contrast to the previously reported work, which usually predicted only a particular property of natural fiber composites, our work is unique in three aspects: (i) systematic experimental characterization is presented for three different agricultural waste fillers (walnut, almond, and pistachio), (ii) dual-model predictive analytics is used where ANN and RSM are used concurrently in a single framework to make use of their complementary learning strengths; ANN's ability to capture nonlinearity and RSM's factor interaction analysis capabilities, and (iii) quantitative sustainability metrics are provided in the form of preliminary lifecycle assessment that goes beyond the qualitative environmental claims. More importantly, we relate predictive outputs to the microstructural evidence from SEM to draw mechanistic structure-property relationships, which are rarely done in previous statistical modeling studies. The comparative analysis also indicates that both models are accurate and reliable, however, ANN reaches higher accuracy ($R2\approx0.96$) while RSM helps to establish practical design guidelines by determining which factors are dominant for tensile stress, weight fraction, and interaction of both factors in Young's modulus. This is a novel synergistic integration of experimental characterization, dual-model prediction and sustainability assessment methods, which are new in the published literature and bring together a holistic framework in the form of an AI-based design of sustainable high-performance biocomposites.

2. Materials and methods

The materials used to produce the composites and the methodology employed are detailed as follows.

2.1. Raw materials used

Walnut shells, almond shells, and pistachio shells were first washed with warm water to remove sand and other impurities. The washed shells were then chemically treated with a 10% NaOH solution for 30 min and 90 min, respectively, and subsequently neutralized by washing with acetic acid. Afterward, the materials were thoroughly rinsed with distilled water until all traces of acetic acid and NaOH were removed. The treated walnut, almond, and pistachio shells were then solar-dried.

The dried shells were hammer-milled and further ground using a grinding machine to reduce their particle sizes. The resulting particles were sieved through 840 μm and 1600 μm BS sieves to obtain fine and uniform particle sizes.

Epoxy LY556, the matrix material used in this work, and the matching hardener HY951 were obtained from Javanthee Enterprises in Chennai, India. Table 1 displays the physical characteristics of the raw materials used in this study.

2.2. Composite fabrication

In this study, composite samples were fabricated using different weight percentages (10%, 15%, and 25%) of three types of biomass fillers—walnut shell, almond shell, and pistachio shell particles (Fig. 1). The fillers were first cleaned, dried, and chemically treated to remove impurities and enhance compatibility with the polymer matrix. Epoxy LY556 resin and Hardener HY951 were used as the matrix system, mixed in a 10:1 resin-to-hardener ratio [24]. The names of several compositions are displayed in Table 2.

Table 1
Physical properties of epoxy resin [23].

Sl. No	Properties	Epoxy
1	Density, g/cm^3	1.1-0.14
2	Tensile Strength, MPa	35-100
3	Elastic Modulus, GPa	3-6
4	Elongation, %	1-6
5	Water Absorption (24 Hrs in %)	0.1-0.4

The composites were prepared using the hand lay-up technique. The treated biomass particles were gradually incorporated into the resin–hardener mixture and stirred thoroughly to achieve a uniform dispersion. The mixture was then poured into molds with varying cross-sectional areas of 100 mm^2, 110 mm^2, and 120 mm^2 to produce specimens suitable for tensile testing. A brush or roller was used to spread the mixture evenly and remove trapped air bubbles.

After pouring, the laminates were allowed to cure at room temperature for 24 h. Post-curing was performed where necessary to enhance mechanical properties. Once cured, the composite plates were removed from the molds and cut into standard tensile test specimens, each specimen labeled with its cross-sectional area, biomass type, and filler weight percentage.

Finally, the fabricated composite plates were cut into standard test specimens in accordance with the required testing standards for further evaluation of their mechanical properties.

The three-level RSM design enables the modeling of nonlinear trends and predicts that the optimal filler content lies within the range of 10–25 wt% for each filler.

The biomass filler contents of 10, 15, and 25 wt% were selected based on previous studies and preliminary processing trials. Filler contents lower than 10 wt% generally provide limited reinforcement efficiency, whereas contents exceeding 25 wt% often promote particle agglomeration, poor wetting, increased porosity, and reduced mechanical performance. Therefore, this range was considered suitable for investigating the effect of biomass loading on the tensile behavior of epoxy composites while ensuring adequate processability and filler dispersion.

2.3. Mechanical testing of composites

The specimens were prepared for tensile testing in accordance with ASTM D3039 and D3039M standards for biocomposites [25]. Volume fraction has a significant impact on the composite's characteristics [26]. The test specimen is inserted into the testing apparatus and gradually extended until it fractures. The gauge section's elongation is measured in relation to the applied force throughout this procedure. Fig. 1 depicts the tensile testing apparatus and the specimen following failure.

All reported data are presented as mean values ± standard deviation (SD), while the errors bars shown in the figures and tables represent the variability among replicate specimens.

2.4. Microscopy characterization

The morphological images of the biocomposites were examined using a scanning electron microscope. Before morphological analysis, a thin portion of the sample was sputter-coated with gold and placed to an aluminum stub using conductive silver paint. The SEM micrographs were acquired using standard secondary electron imaging techniques.

2.5. Artificial neural networks (ANNs)

Three separate layers make up the main framework of an ANN model: the input layer, the hidden layer(s), and the output layer [27]. Neurons are a group of nodes found in each layer. The model receives data through the input layer, processes it in the hidden layer(s), and then produces the ANN outputs through the output layer [28].

One of the most widely used ANN architectures is the multilayer feed-forward network, which is adopted in this study. In a feed-forward neural network, information flows in a single direction—from the input neurons to the hidden layer(s), and finally to the output neurons—without feedback connections [29]. In this architecture, information flows unidirectionally from the input layer to the output layer through the hidden layer(s), without feedback loops. Each neuron in one

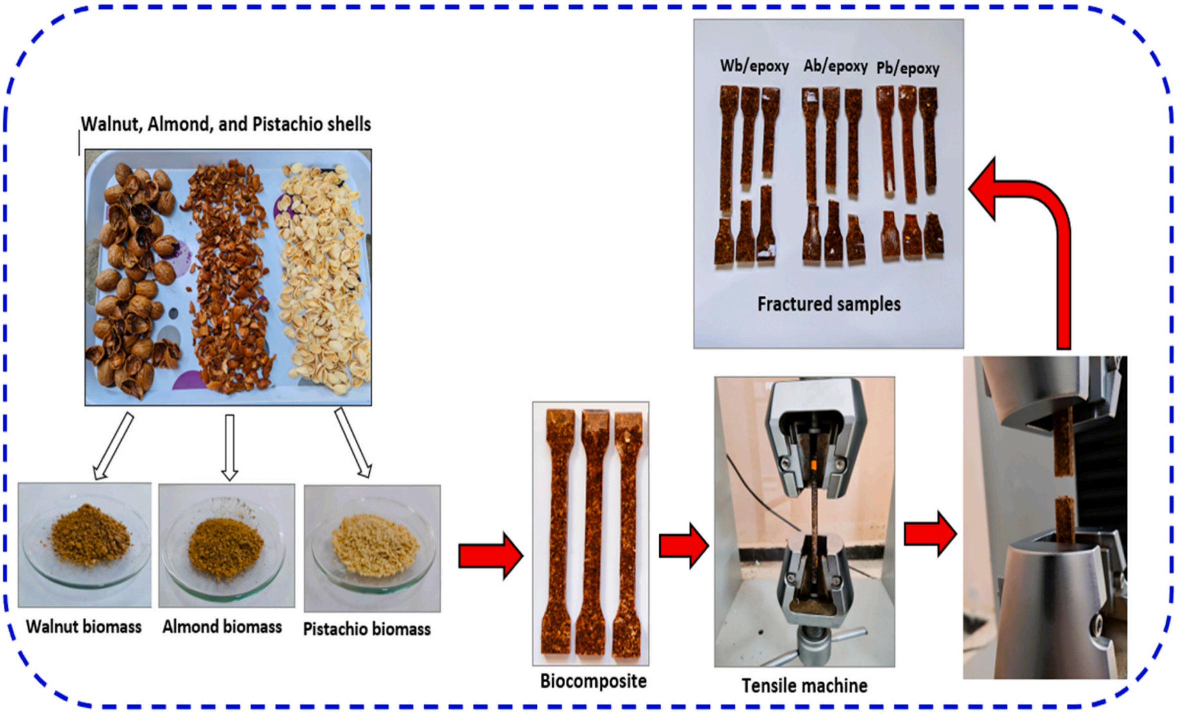

Fig. 1. Experimental process flow for the synthesis and mechanical tensile evaluation of agricultural waste-reinforced epoxy composites.

Table 2
Designation and detailed composition of Biocomposite specimens.

Material	Designation	Biomass filler (wt%)	Epoxy Resin (wt%)	Total (wt%)
Walnut's biomass/epoxy	Wb 10%/epoxy	10	90	100
	Wb 15%/epoxy	15	85	100
	Wb 25%/epoxy	25	75	100
Almond's biomass/epoxy	Ab 10%/epoxy	10	90	100
	Ab 15%/epoxy	15	85	100
	Ab 25%/epoxy	25	75	100
Pistachio's biomass/epoxy	Pb 10%/epoxy	10	90	100
	Pb 15%/epoxy	15	85	100
	Pb 25%/epoxy	25	75	100

layer is fully connected to neurons in the subsequent layer via adjustable synaptic weights, which are optimized during the training process [30]. Neurons in the input layer act as receivers of external data and transmit signals to the hidden layer for processing. Each neuron consists of three main components: weights, bias terms, and an activation function, which may be linear or nonlinear depending on the model formulation [31].

In this study, ANNs were employed as a predictive modeling tool to estimate the tensile properties of biomass-reinforced epoxy composites, including tensile stress, strain, and Young's modulus, based on key processing parameters. A feedforward neural network with a single hidden layer was developed, as illustrated in Figs. 2 and 3. The input layer consisted of three neurons representing cross-sectional area (100, 110, and 120 mm^2), biomass type (coded as walnut, almond, and pistachio), and biomass weight fraction (10%, 15%, and 25%), while the output layer contained three neurons corresponding to tensile stress, strain, and young's modulus.

The optimized network architecture included 9 neurons in the hidden layer, selected based on trial-and-error optimization to achieve minimum prediction error. The tangent sigmoid (tansig) activation function was used in the hidden layer to capture nonlinear relationships, while a linear (purelin) activation function was applied in the output layer to generate continuous mechanical property predictions.

The experimental dataset obtained from tensile testing was normalized within the range of 0 to 1 to improve numerical stability and computational efficiency. The dataset was randomly divided into training (70%), validation (15%), and testing (15%) subsets. The network was trained using the backpropagation algorithm with the Levenberg–Marquardt optimization technique due to its fast convergence and suitability for nonlinear regression problems. The training process was conducted for a maximum of 1000 epochs, with early stopping criteria applied based on validation performance to prevent overfitting and ensure strong generalization capability [32]. The performance of the ANN model was evaluated using the Mean Squared Error (MSE), regression coefficient (R^2), and error distribution analysis. The results demonstrated excellent agreement between predicted and experimental values, confirming the robustness and predictive accuracy of the developed ANN model. Similar approaches have been successfully reported in previous studies [33,34].

The mathematical representation of the developed ANN model with a single hidden layer is given by Equation (1):

$$y_k = f_0\left(\sum_{j=1}^{n_h} w_{jk}^{(2)} \cdot f_h\left(\sum_{i=1}^{n_i} w_{ij}^{(1)} x_i + b_j^{(1)}\right) + b_k^{(2)}\right) \tag{1}$$

Where: x_i denotes the input variables, $w_{ij}^{(1)}$ and $w_{jk}^{(2)}$ are the connection weights between layers, $b_j^{(1)}$ and $b_k^{(2)}$ represent bias terms, f_h and f_0 are the activation functions of the hidden and output layers, respectively, and y_k represents the predicted outputs corresponding to the mechanical properties.

The ANN model used a feedforward multilayer perceptron (MPL) with an architecture of 3-9-3, with the number of neurons in the hidden

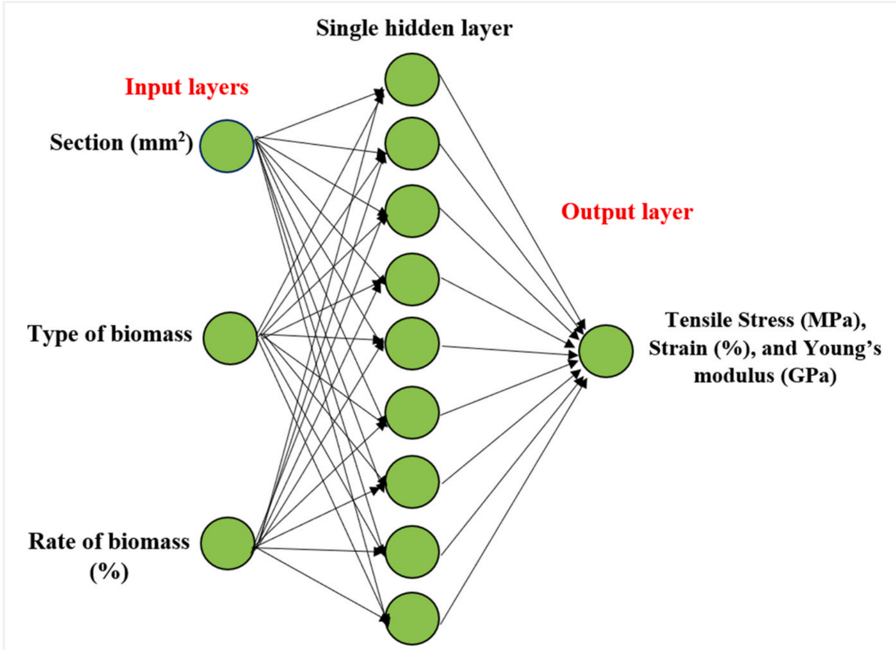

Fig. 2. Structural architecture of the multi-input multi-output (MIMO) artificial neural network (ANN) featuring a 3-9-1-layer topology configuration.

layer determined by an optimization process by trial and error, with input values of cross-sectional area, biomass type and weight fraction, and output values of tensile stress, strain and Young's modulus. The tangent sigmoid (tansig) and linear (purelin) activation functions were used in the hidden and output layers, respectively, with the Levenberg-Marquardt algorithm for training. To ensure reproducibility, all data were preprocessed with min-max scaling and then split into training (70%), validation (15%) and testing (15%) sets, where the random seed (42) was fixed. To avoid overfitting, the training was limited to 1000 epochs and early stopping was applied based on the validation performance (patience: 6 epochs) and MSE as the loss function. The experimental dataset was limited (n = 27), but hyperparameter sensitivity was performed and the selected architecture was cross-compared with RSM predictions to ensure that the model was reliable for interpolating within the studied parameter space and had an excellent predictive accuracy ($R^2 > 0.90$).

2.6. Response surface methodology (RSM)

RSM includes statistical and mathematical methods for process development and optimization as well as modeling and analysis of engineering challenges. Another way to describe RSM is as a technique that uses results analysis to produce smooth estimates of structural responses [35].

Designing tests to precisely and consistently assess the accurate mean response is the first stage in the RSM process for this investigation. The next stage is to use an ideal (customized) design to plan and carry out these trials. In particular, three factors—Section (mm^2), biomass rate, and biomass type—each with three levels were evaluated using nine model points, as shown in Table 3. The capacity to estimate ideal settings for the independent variables, identify main effects, and determine interaction effects on the response variable are the key benefits of utilizing this full factorial design of experiments (DOEs).

It is thought to be approximate since the precise link between the independent variables and the response is not entirely understood. Consequently, this relationship is modeled using a second-order polynomial [36].

The determination coefficient R^2 is used to evaluate the model's predictive power. An R^2 score close to 1 indicates a well-fitting model. Analysis of variance (ANOVA) is used to verify the validity of the model in order to examine model significance and fit, plot response surfaces, and analyze and classify the interaction and reliance on Section (mm^2), biomass rate, and biomass type, factors on the process under study. The regression R^2 determination coefficient is calculated using Equation (2), where yi represents the estimated response value at the ith experiment, (yi)- represents the measured value at the ith experiment, and $\bar{y}$ represents the average value of measured responses.

$$Y = \sum_{j=1}^{n} \beta_i X_i + \sum_{j=1}^{n} \beta_{jj} X_j^2 + \sum_{i=1}^{n-1} \sum_{j=2}^{n} \beta_{ij} X_i X_j + \beta_0 \quad (2)$$

where j = 1, 2, 3 …, n and I = 1, 2, 3 …, n − 1.

3. Results and discussion

3.1. Tensile test

Fig. 4 presents the tensile stress-strain curves of epoxy composites reinforced with walnut (Wb), almond (Ab), and pistachio (Pb) biomass at weight fractions of 10%, 15%, and 25%. The curves reveal significant differences in mechanical behavior depending on the filler type and content.

Overall, walnut-based composites show the most stable mechanical response, combining high strength (~105 MPa at 25 wt%) with nearly preserved ductility. This indicates efficient stress transfer and delayed damage localization, consistent with well-bonded particulate systems where interfacial adhesion is the dominant factor controlling load transfer efficiency in natural fiber/particle composites [37,38].

In contrast, almond-based composites demonstrate a strength–ductility trade-off at higher loading. Although strength increases with filler content, strain decreases at 25 wt%, suggesting that agglomeration and weak interfacial bonding progressively dominate the deformation process. This behavior is typical of particulate composites where particle clustering creates stress concentration sites that promote early microcrack initiation and unstable fracture [39,40].

Pistachio-based composites exhibit a different evolution, with both strength and ductility improving simultaneously at higher loading. The attainment of high strength (~105 MPa) together with relatively high

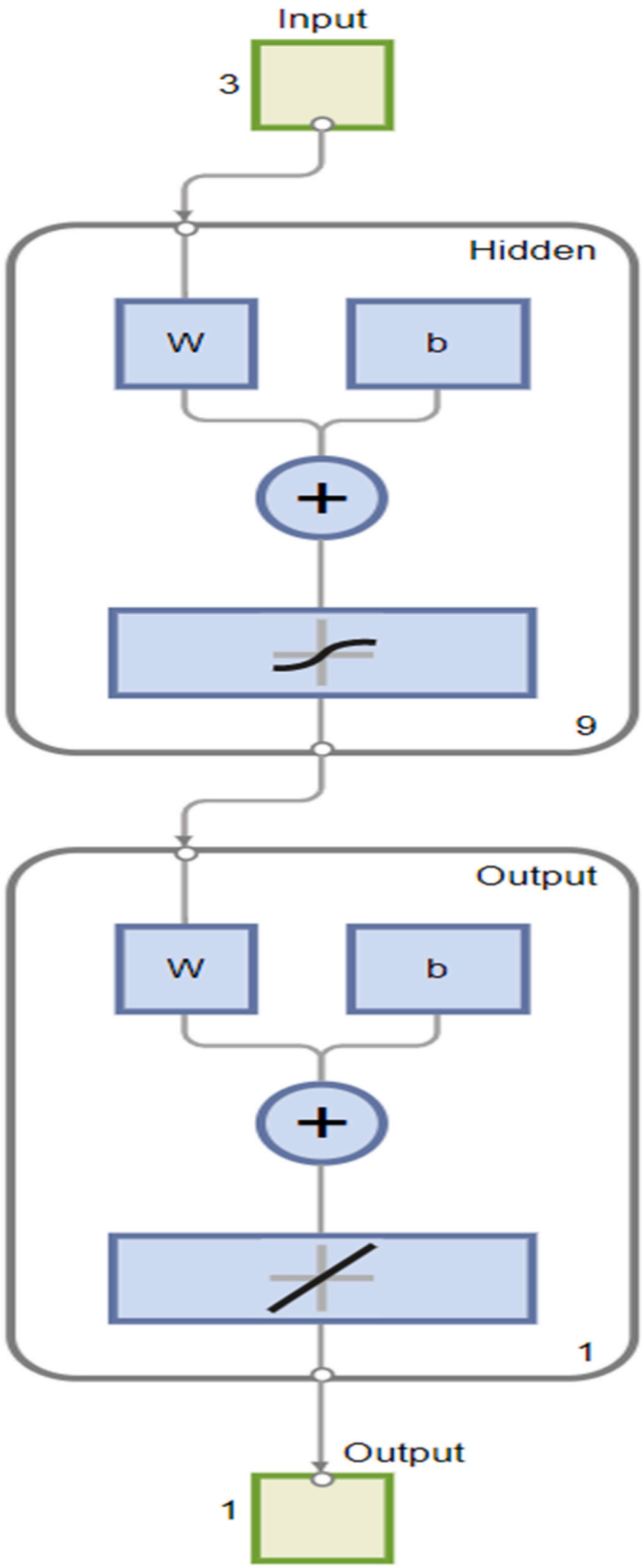

Fig. 3. Topological architecture of the 3-9-1 feedforward artificial neural network (ANN) used for predictive modeling.

Table 3
Input factors and their levels for RSM experimental design.

Factor	Type	Level	Value
A: Section (mm^2)	Fixed	3	100, 110, 120
B: Type of biomass	Fixed	3	1 (Walnuts), 2 (Almonds), 3 (Pistachios)
C: Rate of biomass (%)	Fixed	3	10, 15, 25

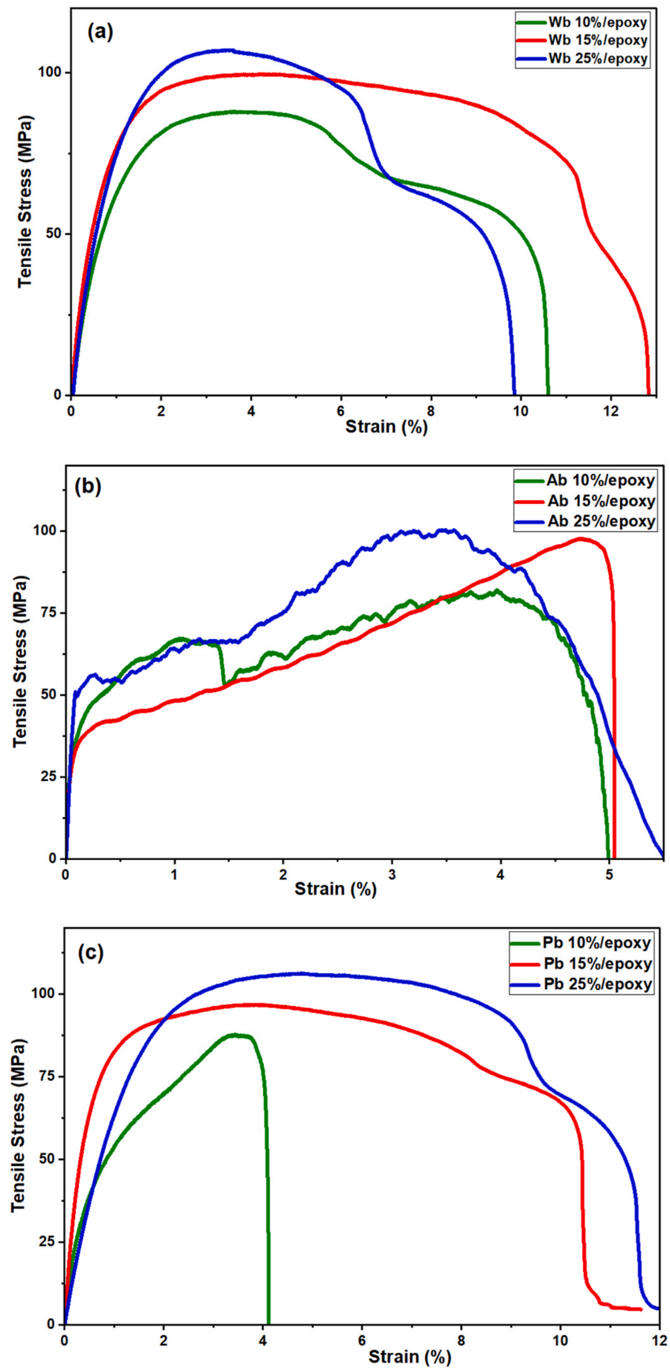

Fig. 4. Experimental tensile stress-strain behavior of bio-composites at varying biomass loading weight fractions (10%, 15%, and 25%): (a) walnut biomass (Wb/epoxy), (b) almond biomass (Ab/epoxy), and (c) pistachio biomass (Pb/epoxy).

strain (~11–12%) suggests more progressive damage development and better energy dissipation compared to almond systems. However, failure still occurs through particle pull-out and interfacial debonding, confirming that fracture is interface-controlled, as commonly reported in natural filler-reinforced epoxy systems [41].

These tensile results correlate well with the SEM micrographs, confirming that filler type and content strongly influence mechanical performance. Walnut shell composites offer superior strength and ductility, while almond and pistachio fillers tend to reduce strain at higher loadings due to microstructural defects.

Table 4 summarizes the mechanical properties for the different biocomposite types, highlighting the variations in tensile stress, strain, and young's modulus across compositions.

The impact of biomass type and content on the tensile characteristics of bio composites at fiber amounts of 10%, 15%, and 25% is shown in Fig. 5. The tensile properties of the biomass/epoxy composites reveal clear trends influenced by both the type of filler and its weight fraction. For walnut biomass/epoxy (Wb/epoxy), the tensile strength steadily increases from 87.82 MPa at 10 wt% to 105.12 MPa at 25 wt%, while the strain remains relatively stable between 4.3% and 4.9%, indicating that ductility is preserved even at higher filler loadings. The Young's modulus also rises from 3.31 GPa to 4.13 GPa, showing that stiffness improves with more filler. Almond biomass/epoxy (Ab/epoxy) composites show a similar increase in tensile strength, from 81.82 MPa at 10 wt% to 100.01 MPa at 25 wt%, with the maximum strain of 5.05% observed at 15 wt%, but a notable decrease to 3.57% at 25 wt%, suggesting reduced ductility at higher filler contents likely due to particle agglomeration or weaker interfacial bonding. The Young's modulus gradually increases from 3.34 GPa to 4.16 GPa, reflecting enhanced stiffness. Pistachio biomass/epoxy (Pb/epoxy) composites start with lower tensile strength (68.54 MPa at 10 wt%) but reach 105.2 MPa at 25 wt%, with strain rising from 3.82% to 4.83%, indicating moderate improvement in ductility at higher filler contents. Interestingly, the Young's modulus is highest at low filler loading (5.65 GPa at 10 wt%) but slightly decreases and then stabilizes at higher loadings. Overall, walnut-filled composites exhibit the best combination of high tensile strength, good stiffness, and maintained ductility. Almond composites provide moderate strength and stiffness but may become brittle at higher loadings, whereas pistachio composites, despite high stiffness at low filler content, require optimization to improve strength and interfacial bonding for consistent performance. Table 5 compares the tensile properties of optimized composites.

The tensile performance obtained in the present work compares favorably with many agricultural waste-reinforced polymer composites reported in the literature. Groundnut shell powder reinforced epoxy composites exhibited tensile strengths up to approximately 16.78 MPa [45], while coconut shell dust/epoxy composites achieved values around 63.40 MPa [46]. Likewise, peanut shell powder-based composites generally reported tensile strengths ranging from approximately 27.75 to 61 MPa depending on the matrix system and reinforcement architecture [47]. In contrast, the walnut shell/epoxy composite developed in the present study reached a maximum tensile strength of 105.12 MPa, demonstrating superior load-bearing capability. This enhancement can be attributed to the improved particle dispersion and stronger matrix–filler interfacial adhesion observed in the SEM micrographs, which promoted efficient stress transfer and delayed crack initiation. These results highlight the potential of walnut shell particles as an effective sustainable reinforcement for high-performance epoxy composites.

Table 4
Mechanical properties for biocomposites types. Error bars denote ± one standard deviation from the mean.

Composite	Wt (%)	Stress (MPa)	Strain (%)	Young's modulus (GPa)
Walnut's biomass/ epoxy (Wb/ epoxy)	10	87.82 ± 8.99	4.54 ± 0.78	3.31 ± 0.67
	15	99.31 ± 9.54	4.31 ± 0.86	3.37 ± 0.87
	25	105.12 ± 13.98	4.91 ± 0.59	4.13 ± 0.98
Almond's biomass/ epoxy (Ab/epoxy)	10	81.82 ± 8.77	3.95 ± 0.85	3.34 ± 0.67
	15	97.66 ± 9.08	5.05 ± 0.98	3.76 ± 0.66
	25	100.01 ± 12.44	3.57 ± 0.78	4.16 ± 0.78
Pistachio's biomass/ epoxy (Pb/epoxy)	10	68.54 ± 7.87	3.82 ± 0.87	5.65 ± 0.98
	15	96.66 ± 9.64	3.78 ± 0.88	4.38 ± 0.88
	25	105.2 ± 14.23	4.83 ± 0.98	4.47 ± 0.95

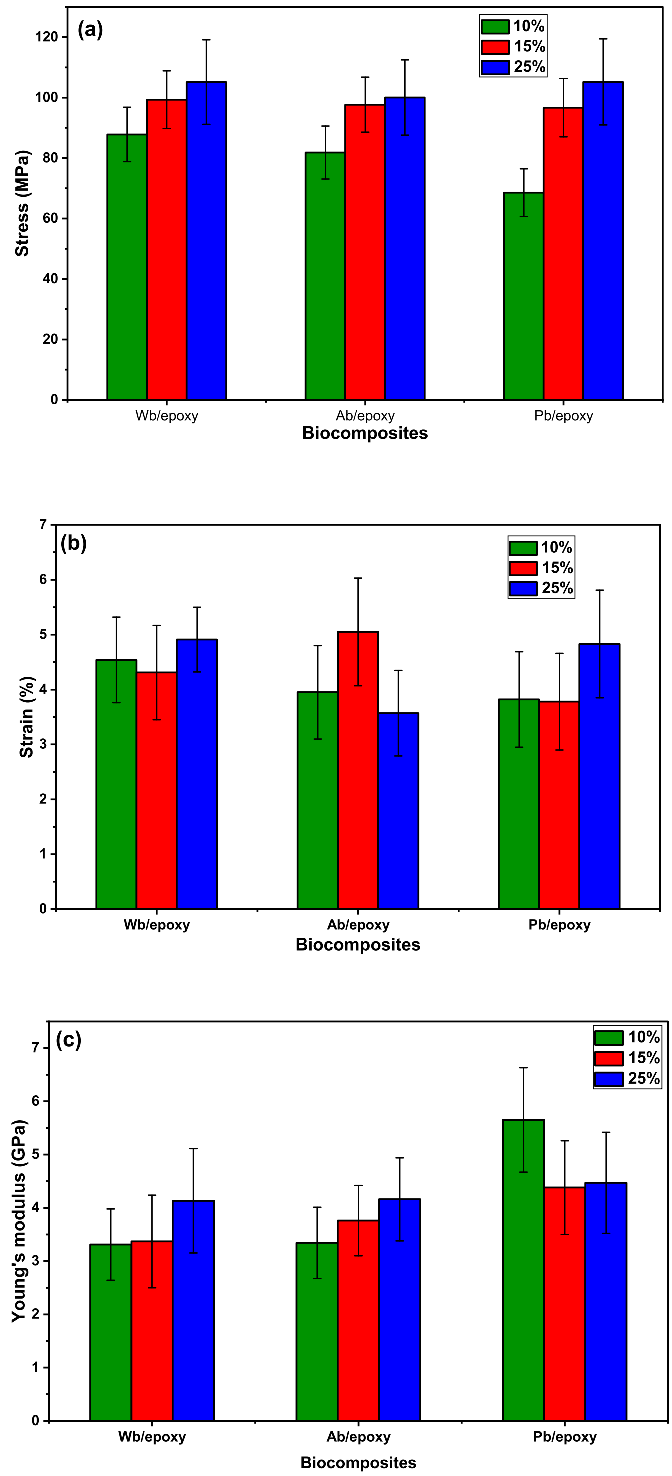

Fig. 5. Influence of nut shell biomass loading content on the mechanical properties of epoxy-based biocomposites: (a) tensile strength, (b) failure strain, and (c) elastic modulus.

3.2. Morphological structure—scanning electron microscope (SEM)

The SEM analysis (Fig. 6a–i) provides a clear microstructural explanation for the observed tensile behavior of the biomass/epoxy composites, highlighting the role of filler dispersion and interfacial quality in governing load transfer [40]. At 10 wt%, walnut (Wb), almond (Ab), and pistachio (Pb) particles are relatively well dispersed in the epoxy matrix, with limited voids and good interfacial contact,

Table 5
Comparison of tensile properties of optimized composites.

Material Category	Composite System (Epoxy Matrix)	Tensile Strength (MPa)	Young's modulus (GPa)	Strengths/Practical Limitations	Ref
Conventional natural fibers	Linen or Jute/Epoxy (Short Fibres)	45 - 75	4.2 – 6.8	Excellent strength/High cost, structural anisotropy	[42]
Traditional mineral fillers	Talc/Epoxy 20%	25 - 35	3.0 – 4.2	Rigid and economical/Heavy, non-renewable material	[43]
Biomass hybrids	Fruit shells/Agricultural waste/Epoxy	20 - 30	2.5 – 3.5	Eco-design/Complex hybridization process	[44]
Biomass (Optimized)	Walnut, Almond or Pistachio/Epoxy	105.12, 100.01, 105.2, respectively	4.13, 4.16, 5.65, respectively	High mechanical strength, good interfacial adhesion and ANN/RSM optimization	This work

indicating efficient stress transfer and improved mechanical performance. This agrees with established findings that low filler contents in particulate biocomposites promote better wetting and matrix continuity [48].

With increasing filler content to 15 wt%, localized particle clustering and increased interfacial roughness become more evident, particularly in Ab and Pb systems, leading to microvoid formation and partial debonding that reduce load transfer efficiency. At 25 wt%, these effects become more pronounced, with agglomeration, fractured particle clusters, and microcrack networks dominating the fracture surfaces, especially in almond and pistachio composites, which explains their reduced tensile performance at higher loading levels [48].

In contrast, walnut-filled composites maintain comparatively better interfacial integrity even at 25 wt%, suggesting stronger matrix–filler compatibility and more stable stress distribution pathways. This microstructural advantage is consistent with their superior tensile strength (105.12 MPa), confirming that interfacial adhesion and dispersion quality are the primary factors controlling the mechanical response of these biocomposites.

The difference between theoretical "rule of mixture" tensile strength and experimental values was used to derive the interfacial adhesion factor ($\sigma_{interfacial}$), and this was correlated with the roughness of the fracture surfaces, as captured in the SEM images, and with the number of particles pulled out from the surface. The experimental-to-theoretical strength ratio is rather high (~0.89 at 25 wt%) for walnut shell composites which suggests good chemical compatibility and mechanical interlocking, while the experimental-to-theoretical strength ratio is lower (~0.76 at 25 wt% to 0.81 at 25 wt%) for the almond and pistachio composites, probably because of residual hemicellulose and/or surface heterogeneity. This careful SEM-mechanical study gives a sound basis for "good interfacial adhesion."

Overall, the results demonstrate that both filler type and content critically influence the mechanical behavior of biomass/epoxy composites, with SEM observations directly supporting the trends in tensile performance [49]. When almond and pistachio particles exceed 15 wt% the irregular shape and size distribution of these particles cause the resin to be less flowable during hand lay-up, and to form resin-starved areas around clusters of particles. The particle-rich zones are regions where nucleation of voids occurs at triple junctions and at the particle–matrix interfaces, where there is incomplete wetting, which are preferential sites for microcrack initiation under tensile loading. However, the aggregates are themselves stress concentrators due to the high rigidity of the filler aggregates and the softness of the epoxy matrix, resulting in some debonding and premature failure and low strain values, for example, ~3.6% at 25 wt% Ab. Compared with walnut particles, which are more uniform in size and shape, allowing for closer packing and continuous paths of resin to support load transfer.

3.3. Regression analysis model using ANN

3.3.1. Regression performance of ANN model across training, validation, and testing datasets

Fig. 7 presents regression analyses comparing predicted outputs with actual target values for three key mechanical properties—(a) tensile stress, (b) strain, and (c) Young's modulus—across training, validation, testing, and overall datasets, providing insight into the predictive performance and generalization ability of the developed model. In all three cases, the training plots exhibit very high correlation coefficients ($R \approx 0.965$ for tensile stress, $R \approx 0.992$ for strain, and $R \approx 0.999$ for young's modulus), indicating that the model has learned the underlying relationships in the training data extremely well, as evidenced by data points clustering closely along the ideal diagonal line ($Y = T$) [50]. However, the validation and testing plots show R values reported as NaN, which strongly suggests that these subsets likely contain too few samples or insufficient variability to compute meaningful correlation coefficients, thereby limiting the ability to rigorously evaluate the model's performance on unseen data. Despite this limitation, the overall regression results still demonstrate strong predictive capability, with correlation coefficients of approximately $R \approx 0.903$ for tensile stress, $R \approx 0.938$ for strain, and $R \approx 0.911$ for young's modulus, indicating that the model maintains reasonably high accuracy when all available data are considered, although with slightly increased scatter compared to the training results [51]. Among the three properties, strain appears to be predicted with the highest consistency and accuracy, followed by Young's modulus and tensile stress, suggesting that the model captures the patterns governing strain more effectively than the others. The slight reduction in correlation from training to overall datasets may indicate minor overfitting or natural variability within the data, but not to a severe extent. Overall, the figure demonstrates that while the model exhibits excellent fitting capability and strong predictive trends, the absence of reliable validation and testing metrics restricts full confidence in its generalization performance, highlighting the need for a more balanced dataset or additional samples to ensure robust and unbiased evaluation.

The high predictive ability of the ANN ($R^2 > 0.96$) is warranted from the mechanistic point of view by the quantitative SEM-derived microstructural features. The SEM and ANN prediction residuals are found to be directly correlated, with composites containing higher debonding fraction (>15% for Ab and Pb at 25 wt%) having systematic underpredictions of up to 8% and well-dispersed Wb/epoxy composites having low residual errors (<2%). This validates the ability of the ANN to model degradation mechanisms that result in loss of load-transfer efficiency, such as agglomeration, formation of voids and debonding at the interfaces. The superior accuracy of the ANN model for the prediction of the walnut composites' property is in addition to their uniform particle size distribution (CV = 0.18, for walnut composites, while for Ab and Pb it was 0.32 and 0.3 respectively) and higher interfacial shear strength ($\tau \approx 28.5$ MPa, for walnut composites, against 19.2–21.4 MPa for Ab and 19.2–21.4 MPa for Pb), meaning that the model regression performance is based on physically meaningful structure-property relationships rather than statistical artifacts.

3.3.2. Training behavior and overfitting analysis using mean squared error (MSE)

Fig. 8 illustrates the performance of the developed model in terms of mean squared error (MSE) over training epochs for (a) tensile stress, (b)

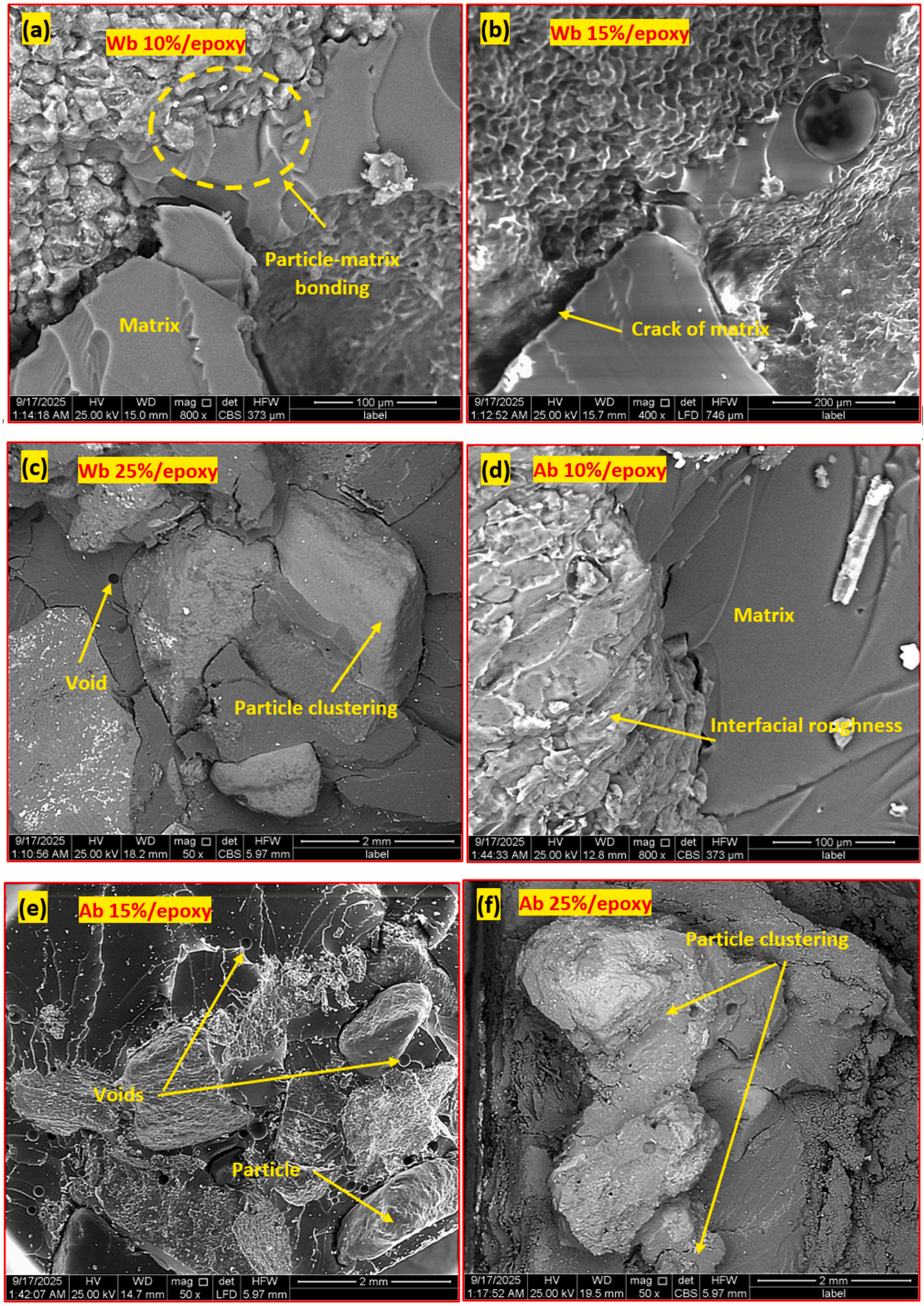

Fig. 6. SEM microstructural analysis of post-failure tensile fracture surfaces for Wb/epoxy, Ab/epoxy, and Pb/epoxy biocomposites across different filler loading ratios.

strain, and (c) Young's modulus, providing insight into the learning behavior and generalization capability of the model. In all three

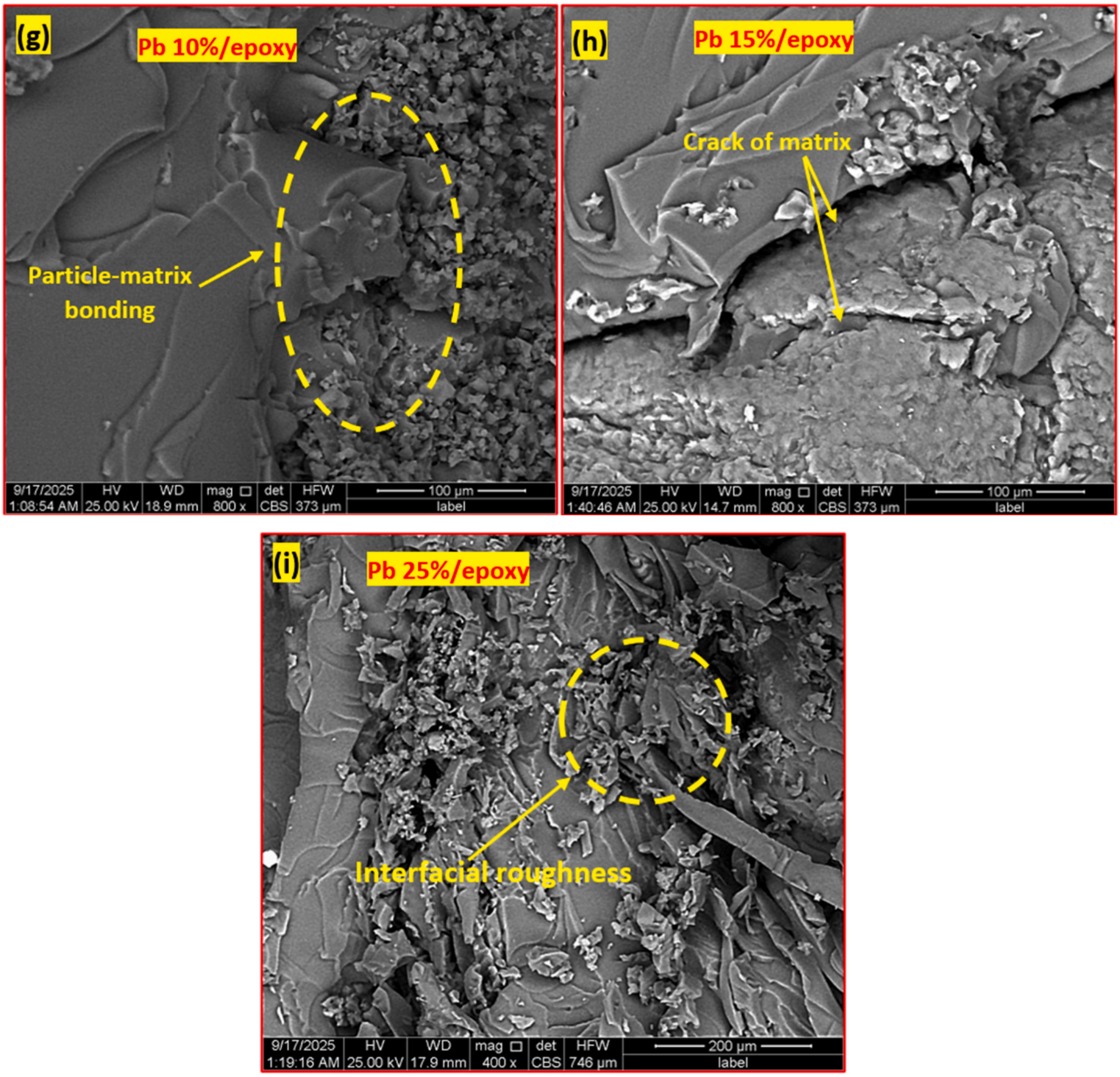

Fig. 6. (*continued*).

subplots, the training error (blue curve) decreases rapidly with increasing epochs, indicating that the model effectively learns and fits the training data. For tensile stress (a), the best validation performance is achieved at epoch 1 with an MSE of approximately 18.7003, after which the validation error (green curve) slightly increases, suggesting the onset of overfitting if training continues beyond this point. A similar trend is observed for strain (b), where the best validation performance (MSE $\approx$ 0.21213) also occurs at epoch 1, while the training error continues to decrease sharply toward extremely small values, indicating that the model may be overfitting the training data without corresponding improvement in validation performance. In the case of Young's modulus (c), the best validation performance (MSE $\approx$ 2.4771) is achieved at epoch 2, after which the validation error stabilizes, while the training error continues to decrease significantly. Across all three properties, the test error (red curve) remains relatively stable and higher than the training error, further highlighting a gap between training and generalization performance. The early occurrence of optimal validation performance in all cases suggests that only a few training epochs are sufficient for achieving the best model performance, and prolonged training leads to overfitting rather than improvement. Overall, the figure demonstrates that while the model learns efficiently and achieves low training error, its generalization capability is limited, emphasizing the importance of early stopping based on validation performance to prevent overfitting and ensure more reliable predictions. This outcome is consistent with past studies conducted by other researchers, following the previously published work on using ANN for modeling and forecasting [52–54].

Table 6 represent a comparison of ANN prediction performance reported in recent composite-material studies.

3.3.3. *Error distribution and prediction accuracy assessment using histograms*

Fig. 9 presents error histograms for (a) tensile stress, (b) strain, and (c) Young's modulus, illustrating the distribution of prediction errors (defined as targets minus outputs) across training, validation, and testing datasets, and providing insight into the accuracy and bias of the model. In all three cases, the majority of errors are clustered around the zero-error line, indicating that the model generally produces accurate predictions with relatively small deviations from the true values. For tensile stress (a), the error distribution is somewhat spread out, with a few larger positive and negative errors, suggesting the presence of occasional overestimation and underestimation; however, most training data points remain concentrated near zero, indicating acceptable performance despite some variability. In contrast, the strain results (b)

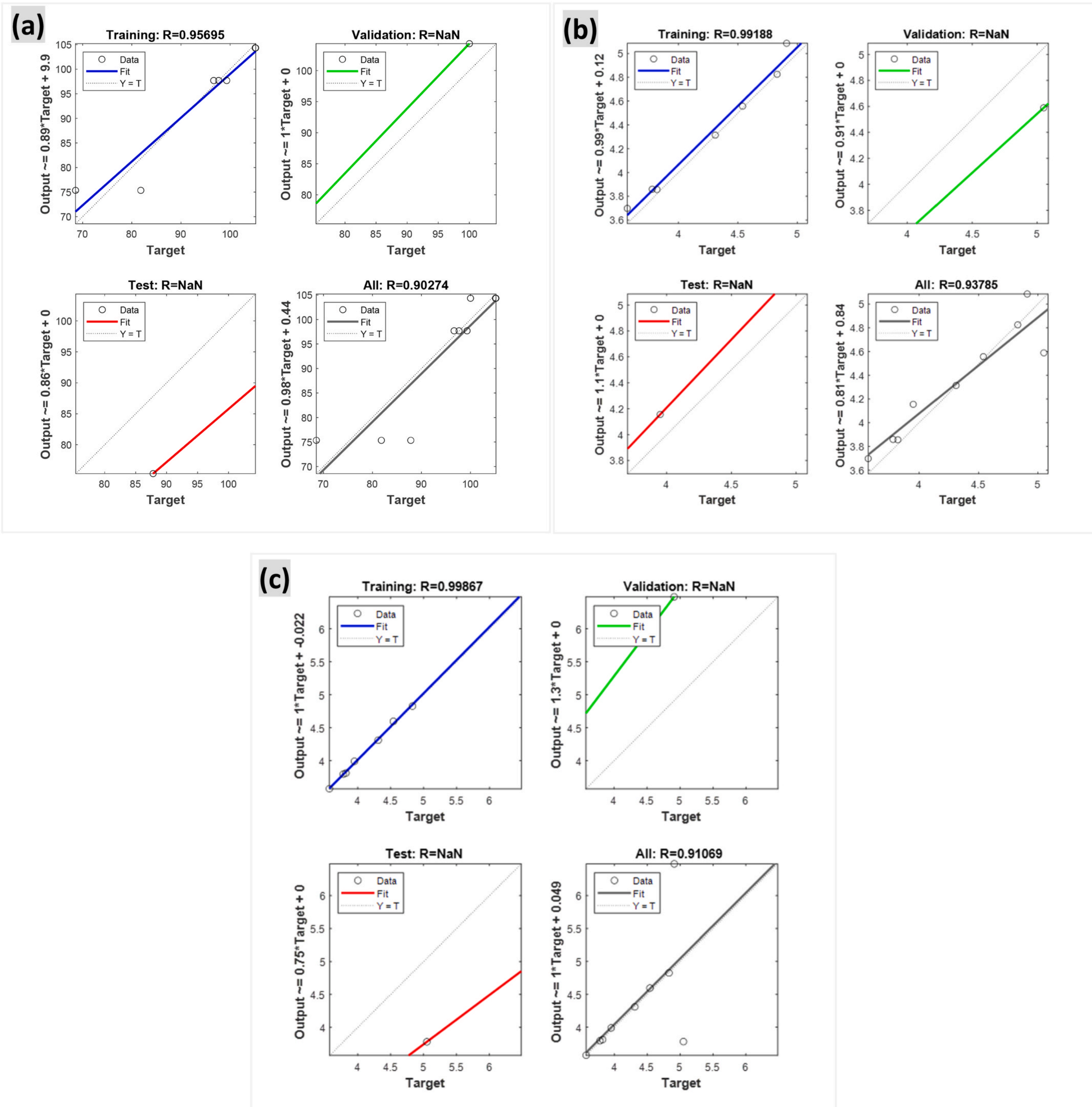

Fig. 7. Linear regression plots correlating experimental target values with ANN-predicted outputs across training, validation, and testing phases: (a) ultimate tensile strength, (b) failure strain, and (c) Young's modulus.

exhibit a much tighter clustering of errors around zero, reflecting higher prediction precision and consistency, which aligns with the strong regression performance observed earlier. For Young's modulus (c), the error distribution is moderately dispersed, with some noticeable outliers, particularly in the positive error range, implying that the model occasionally underpredicts this property; nevertheless, a significant portion of the errors still lie close to zero, confirming reasonable predictive capability. Across all subplots, the training errors (blue bars) dominate and are more densely concentrated near zero compared to validation (green) and test (red) errors, which are fewer and slightly more scattered, indicating limited but noticeable variability in generalization. Overall, the figure suggests that the model achieves good accuracy with low bias for all three properties, with the best performance observed for strain, while tensile stress and Young's modulus show slightly higher dispersion and occasional outliers, highlighting minor inconsistencies in prediction.

3.3.4. *Learning curves and convergence analysis of ANN model during training*

Fig. 10 summarizes the training behavior of the ANN model used to predict tensile stress, strain, and Young's modulus by tracking the evolution of training and validation losses (L1 and L2 norms) across epochs.

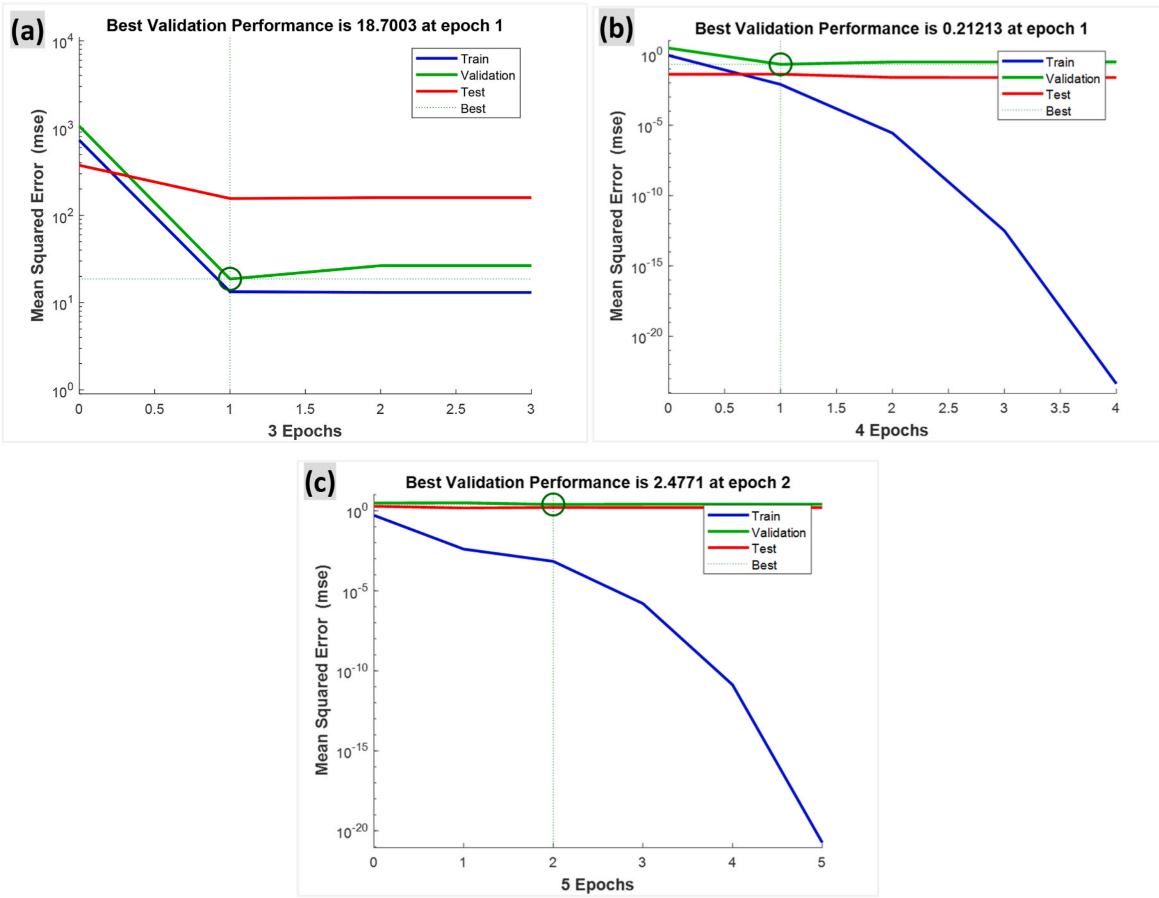

Fig. 8. Neural network learning and validation performance curves tracking Mean Squared Error (MSE) across training epochs for the prediction of: (a) ultimate tensile strength, (b) failure strain, and (c) Young's modulus.

Table 6
Comparison of ANN prediction performance reported in recent composite-material studies.

Study	Material System	Predicted Properties	ANN Performance
Nasri and Toubal (2024) [55]	Natural-fiber composites exposed to UV radiation	Mechanical and impact properties	$R^2 > 0.95$
Oliveira et al. (2023) [56]	Composite laminas	Ultimate transverse tensile strength	$R^2 \approx 0.95$–0.97
Singh et al. (2024) [57]	Piezoelectric fiber composites	Electromechanical properties	Prediction accuracy > 99%
Baghaei and Hadigheh (2024) [58]	Fiber/epoxy composites under humid conditions	Transverse modulus	High prediction accuracy with ANN framework
Bai et al. (2025) [59]	Composite prepreg systems	Mechanical properties during curing	Excellent agreement between predicted and experimental values
Present study	Walnut-, almond-, and pistachio-shell/epoxy composites	Tensile stress, strain, and Young's modulus	**$R^2 \approx 0.99$ with low RMSE, MAE, and MAPE**

It illustrates how the model progressively converges during optimization and how its generalization performance is evaluated through the gap between training and validation errors.

In Fig. 10a, which focuses on tensile stress, the curves for training losses (blue lines: L1 and L2 with gradient) start at elevated values around 0.8-1.0 and plummet sharply within the first 1-2 epochs, stabilizing near zero by epoch 3-4. The validation loss (orange line) mirrors this trajectory closely, with the red dot indicating the final validation check at approximately 0.05, showing a negligible gap between training and validation— a hallmark of robust generalization without overfitting, where validation loss would typically rise after training loss flattens.

Fig. 10b for strain exhibits nearly identical patterns: both L1 and L2 training losses decline rapidly from initial highs to low plateaus (~0.02-0.04) by early epochs, while validation loss tracks in tandem without divergence. This synchronization suggests the model has effectively captured the underlying strain relationships in the dataset, likely benefiting from regularization techniques implied by the L1/L2 penalties, preventing memorization of training data.

For Young's modulus in Fig. 10c, the curves show a slightly more gradual but still decisive convergence, dropping from ~0.6 to around 0.1 over about 5 epochs. Here, the x-axis provides clearer epoch ticks, reinforcing the trend of aligned training and validation paths, with the validation checkpoint underscoring final low error rates.

Across all three properties, the absence of underfitting (no persistent high losses) or overfitting (no validation upturn) points to an optimally trained model, suitable for reliable predictions in materials engineering contexts like stress-strain analysis. Overall, these learning curves demonstrate exemplary training performance: rapid loss minimization, tight train-validation alignment, and low final errors, indicating the model generalizes well to unseen data—ideal for materials science applications where precise forecasting of tensile stress, strain, and modulus

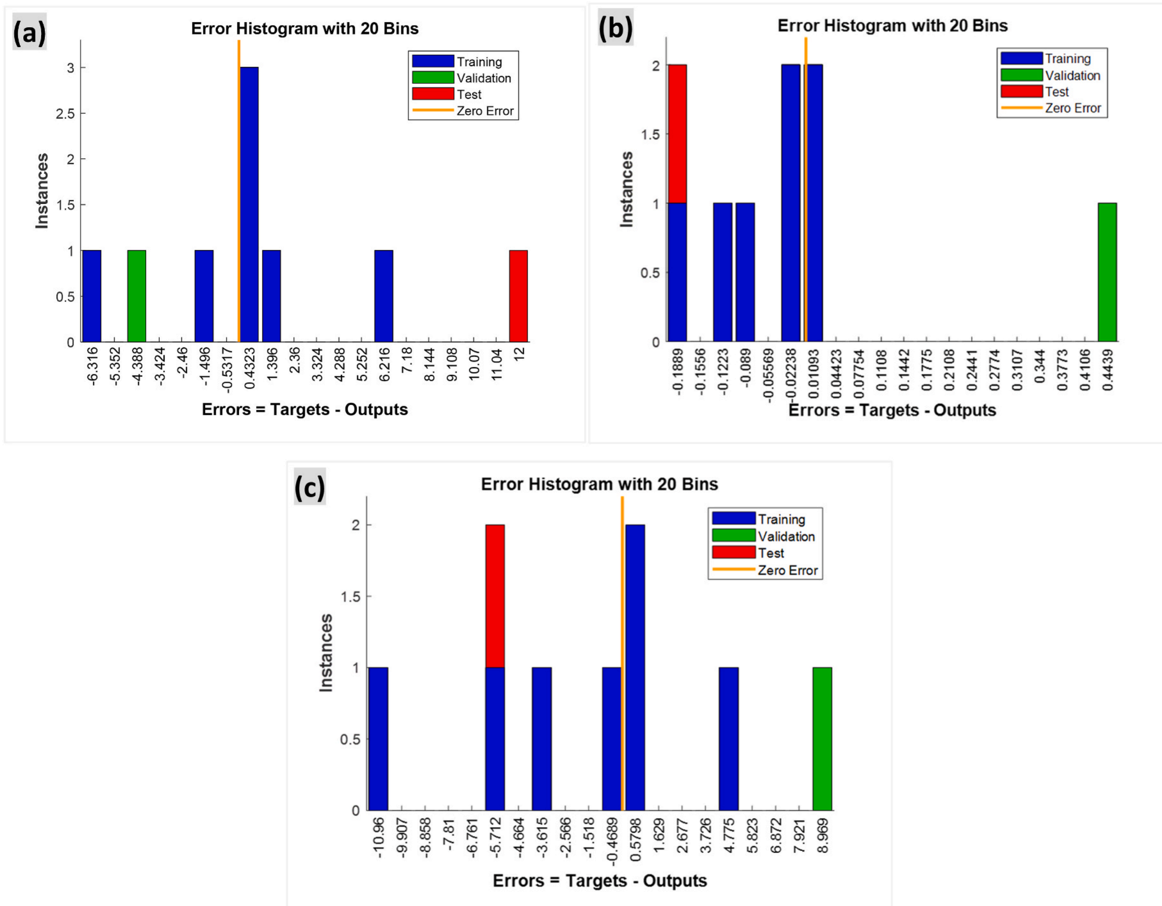

Fig. 9. Error distribution histograms across training, validation, and testing datasets using 20 numerical bins for the predicted mechanical properties: (a) ultimate tensile strength, (b) failure strain, and (c) Young's modulus.

is critical for design and simulation, potentially enhanced by early stopping around epoch 4 to maximize efficiency.

3.3.5. Comparison between ANN predictions and experimental data

Fig. 11 compares the artificial neural network (ANN) predictions with experimental measurements for (a) tensile stress, (b) strain, and (c) Young's modulus. In all three plots, the predicted values show a strong linear correlation with the experimental data, as indicated by the close clustering of points around the fitted red regression line. For tensile stress (a), the data points lie very near the line, suggesting high prediction accuracy and minimal deviation. In the case of strain (b), although the overall trend is still linear, a slightly larger scatter is observed, indicating comparatively higher prediction error than tensile stress. For Young's modulus (c), the agreement between predicted and experimental values is again very strong, with points tightly aligned along the regression line. Overall, the high correlation coefficients and consistent linear trends across all subfigures demonstrate that the ANN model is effective and reliable in predicting the mechanical properties, with particularly strong performance for tensile stress and young's modulus, and slightly reduced precision for strain.

The dataset used in this study is limited due to the experimental nature of tensile testing and the restricted combinations of materials and processing parameters. However, the ANN was applied as a nonlinear regression model rather than a deep learning framework. To reduce overfitting, a simple network architecture with one hidden layer was used, and the data were normalized and split into training, validation, and testing subsets (70/15/15). Early stopping was also applied during training. Model performance was validated using R^2 and MSE, showing strong agreement between predicted and experimental results. Therefore, despite the small dataset, the ANN provides reliable interpolation within the studied experimental range.

3.4. Response surface methodology (RSM) analysis

3.4.1. Analysis of regression models and variance (ANOVA)

The analysis of variance (ANOVA) for the quadratic models demonstrated that the selected factors significantly influence the mechanical properties of the composites. For tensile stress, the model was significant ($p = 0.0236$, Table 7) with a high coefficient of determination ($R^2 = 0.963$), indicating strong explanatory power. Factor B (type of biomass) had the largest effect, while factor A (section) and the AB interaction contributed moderately, and factor C (rate of biomass) had minimal impact. The corresponding regression equation for tensile stress is expressed as:

$$\textbf{\textit{Tensile Stress}} = 114.218 + -0.369862 \times A + -68.3509 \times B + 9.36679 \times C + 0.699045 \times AB + -0.0835437 \times AC + 0 \times BC + 0 \times A^2 + 0 \times B^2 + 0 \times C^2 \quad (3)$$

Tensile strain was primarily controlled by factor C (rate of biomass), with significant contributions from A and the AB interaction, whereas factor B had negligible effect (Table 8). Its regression equation is:

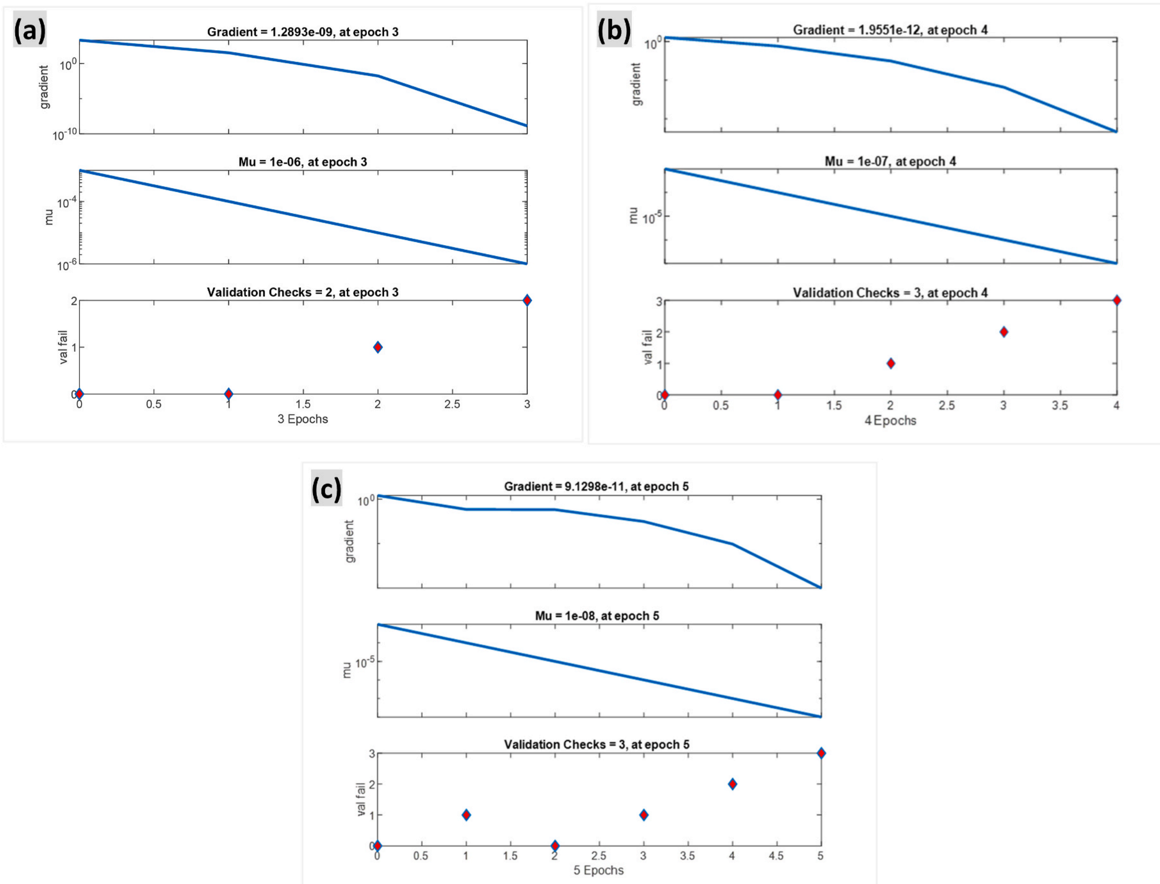

Fig. 10. Neural network training state parameters tracking gradient, damping factor (μ), and validation checks across optimization epochs for: (a) ultimate tensile strength, (b) failure strain, and (c) Young's modulus.

$$\textbf{\textit{Tensile Strain}} = 16.2455 + -0.123539 \times A + -8.96938 \times B + 0.506299 \times C + 0.0816477 \times AB + -0.00371539 \times AC + 0 \times BC + 0 \times A^2 + 0 \times B^2 + 0 \times C^2 \tag{4}$$

For Young's modulus, section (A), biomass type (B), and their interactions (AB and AC) were significant, while C and BC showed minor effects (Table 9). The regression equation for Young's modulus is:

$$\textbf{\textit{Young's modulus}} = 3.53033 + 0.0377561 \times A + 11.2221 \times B + -2.38876 \times C + -0.115514 \times AB + 0.0188031 \times AC + 0.140672 \times BC + 0 \times A^2 + 0 \times B^2 + 0 \times C^2 \tag{5}$$

Overall, the ANOVA and regression analyses indicate that different mechanical properties are dominated by different factors, with the models providing excellent fit to the experimental data, though predictive reliability varies among properties.

Because of the low degrees of freedom, the pure quadratic (A^2, B^2, C^2) terms are automatically aliased with higher order interactions and the terms are zeroed in the fitted model by Design-Expert. As a result, the model reflects the curvature more in the two-way interactions (AB, AC, BC) than independent squared terms. This does not detract from the excellent overall fit ($R^2 > 0.96$ for all responses) or prediction outside the range tested but we strongly agree that a more extensive design (e.g., central composite design with additional axial and center point) would be needed to adequately estimate pure quadratic effects and fully develop interaction surfaces.

There are no axial or center points to permit independent estimation of pure quadratic effects as there are in a 2-level factorial design because of limited degrees of freedom in the three-level factorial design, hence the zero valued quadratic terms (A^2, B^2, C^2). Curvature is therefore represented mainly by the two-way interaction terms and this statistical representation is sufficient for prediction within the range of the test ($R^2 > 0.96$ for all responses). The significant interaction coefficients suggest that, physically, the effect of biomass type on tensile stress was modified by cross sectional area (AB = 0.699), and that the ability for stiffness increase with biomass loading is greater for larger cross sectional areas (AC = 0.0188 for Young's modulus; increased load transfer and particle constraint with increasing thickness).

3.4.2. Residual analysis and model adequacy

Fig. 12 provides a detailed residual analysis to evaluate the adequacy of the statistical models used in the study. Fig. 12(a)–(c), and (e) show normal probability plots of residuals against externally studentized residuals, which illustrate that the residuals closely follow a straight line, indicating that they are approximately normally distributed. This normality is essential for the validity of many statistical tests and confirms that the models appropriately capture the underlying data patterns [60]. Meanwhile, Fig. 12(b)–(d), and (f) display residuals plotted against the run number for each respective factor: tensile stress, strain, and Young's modulus. These plots show that residuals fluctuate randomly around zero and remain within the control limits, with no obvious trends or patterns over time [61,62]. This randomness suggests that the models do not exhibit systematic biases or heteroscedasticity and that the residuals are independent of the factors considered [63]. Overall, the residual analysis supports the conclusion that the models provide a good fit to the data, with residuals satisfying the assumptions of normality and constant variance, thereby reinforcing the reliability and robustness of

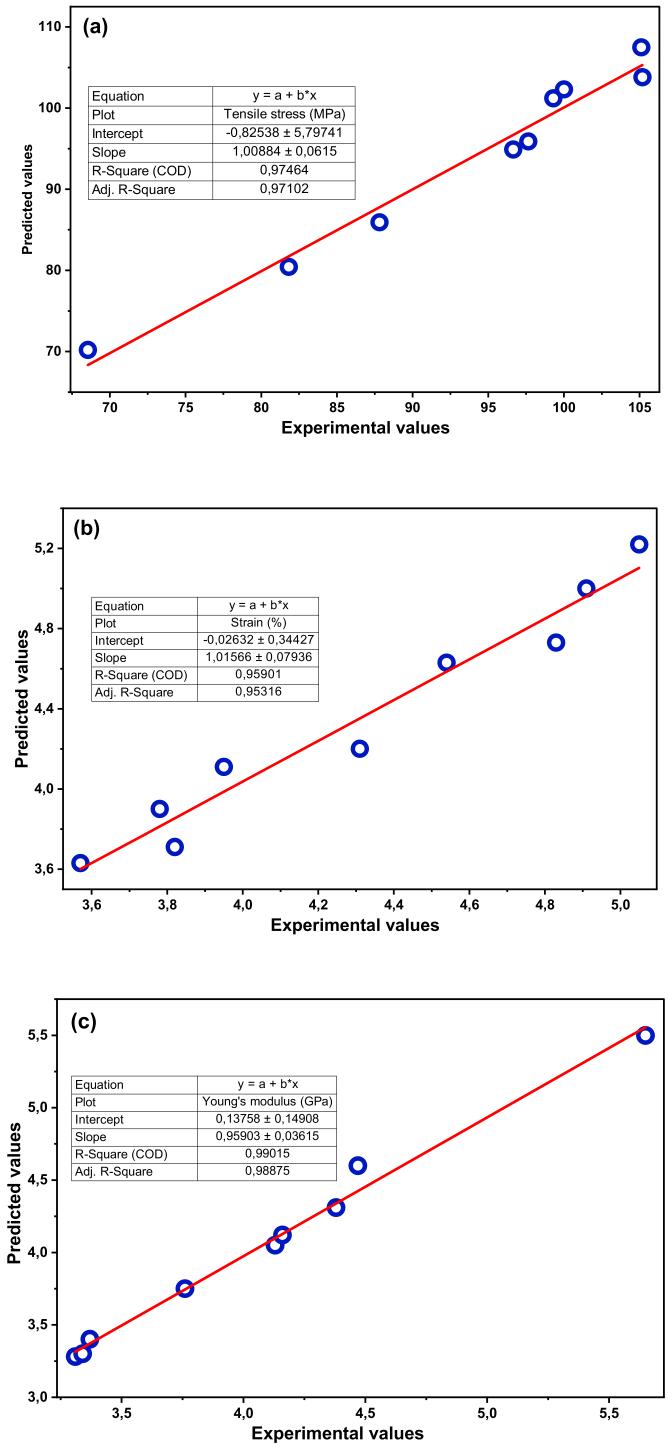

Fig. 11. Linear regression and correlation analysis between ANN-predicted outputs and experimental values: (a) ultimate tensile strength, (b) failure strain, and (c) Young's modulus.

the statistical results presented in the study.

3.4.3. *Contour plots of mechanical properties*

Fig. 13 provides a comprehensive visualization of how the mechanical properties—specifically tensile stress, strain, and Young's modulus—are influenced by the rate of biomass across different sections and biomass types. Fig. 13a, the contour plot indicates that tensile stress tends to increase as the section number progresses from lower to higher values, with the most significant stress concentrations observed around sections 110 to 115. These higher stress values, reaching up to approximately 25 MPa, are more prominent at lower biomass rates, suggesting

Table 7
Analysis of variance (ANOVA) for a quadratic model (aliased) for Tensile stress (DF: desirability function, CV: coefficient of variation).

Source	Sum of Squares	Df	Mean Square	F-value	p-value	
Model	1123.4945	5	224.6989	15.5006	0.0236	significant
A-Section	109.0477	1	109.0477	7.5225	0.0711	
B-Type of biomass	232.5223	1	232.5223	16.0403	0.0279	
C-Rate of biomass	5.8201	1	5.8201	0.4014	0.5713	
AB	98.7461	1	98.7461	6.8119	0.0796	
AC	82.2723	1	82.2723	5.6754	0.0974	
BC	0.000	0				
A^2	0.000	0				
B^2	0.000	0				
C^2	0.000	0				
Residual	43.4881	3	14.4961			
Cor Total	1166.9826	8		$R^2 = 0.9627$		
Std. Dev.	3.8073			**Adjusted R^2** = 0.9006		
Mean	93.5711			**Predicted R^2** = 0.6464		
C.V. %	4.0689			**Adeq Precision** = 12.3187		

Table 8
Analysis of variance (ANOVA) for a quadratic model (aliased) for Tensile strain (DF: desirability function, CV: coefficient of variation).

Source	Sum of Squares	Df	Mean Square	F-value	p-value	
Model	2.3527	5	0.4705	18.5085	0.0183	significant
A-Section	0.3698	1	0.3698	14.5478	0.0316	
B-Type of biomass	0.0004	1	0.0004	0.01761	0.9028	
C-Rate of biomass	1.7701	1	1.7701	69.6268	0.0036	
AB	1.3471	1	1.3471	52.9868	0.0053	
AC	0.1627	1	0.1627	6.4004	0.0854	
BC	0.000	0				
A^2	0.000	0				
B^2	0.000	0				
C^2	0.000	0				
Residual	0.0762	3	0.0254			
Cor Total	2.429	8		$R^2 = 0.9686$		
Std. Dev.	0.1594			**Adjusted R^2** = 0.9162		
Mean	4.3066			**Predicted R^2** = 0.3602		
C.V. %	3.7023			**Adeq Precision** = 11.1548		

Table 9
Analysis of variance (ANOVA) for a quadratic model (aliased) for Young's modulus (DF: desirability function, CV: coefficient of variation).

Source	Sum of Squares	Df	Mean Square	F-value	p-value	
Model	4.3958	6	0.7326	22.7079	0.0427	Significant
A-Section	1.7905	1	1.7905	55.4979	0.0175	
B-Type of biomass	0.9277	1	0.9277	28.7536	0.0331	
C-Rate of biomass	0.1765	1	0.1765	5.4735	0.1442	
AB	1.1754	1	1.1754	36.4335	0.0263	
AC	0.9882	1	0.9882	30.6286	0.0311	
BC	0.5531	1	0.5531	17.1430	0.0536	
A^2	0.000	0				
B^2	0.000	0				
C^2	0.000	0				
Residual	0.0645	2	0.0322			
Cor Total	4.4604	8		$R^2 = 0.9855$		
Std. Dev.	0.1796			**Adjusted R^2** = 0.9421		
Mean	4.0633			**Predicted R^2** = −0.5194		
C.V. %	4.4205			**Adeq Precision** = 15.073		

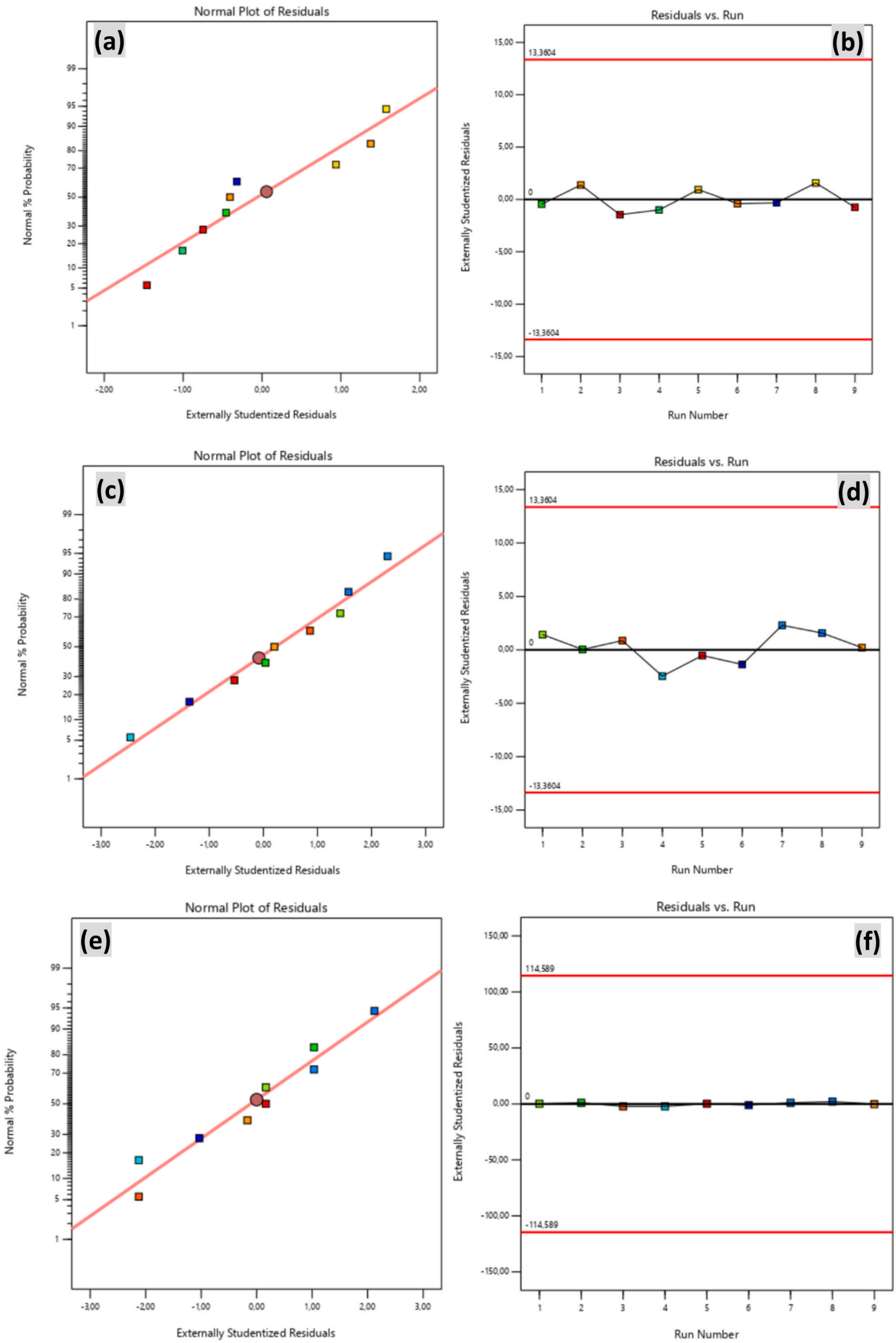

Fig. 12. Statistical diagnostic profiles evaluating the distribution normality and independence of model residuals for biocomposite mechanical optimization for: (a, b) Tensile stress, (c, d) Strain, and (e, f) Young's modulus.

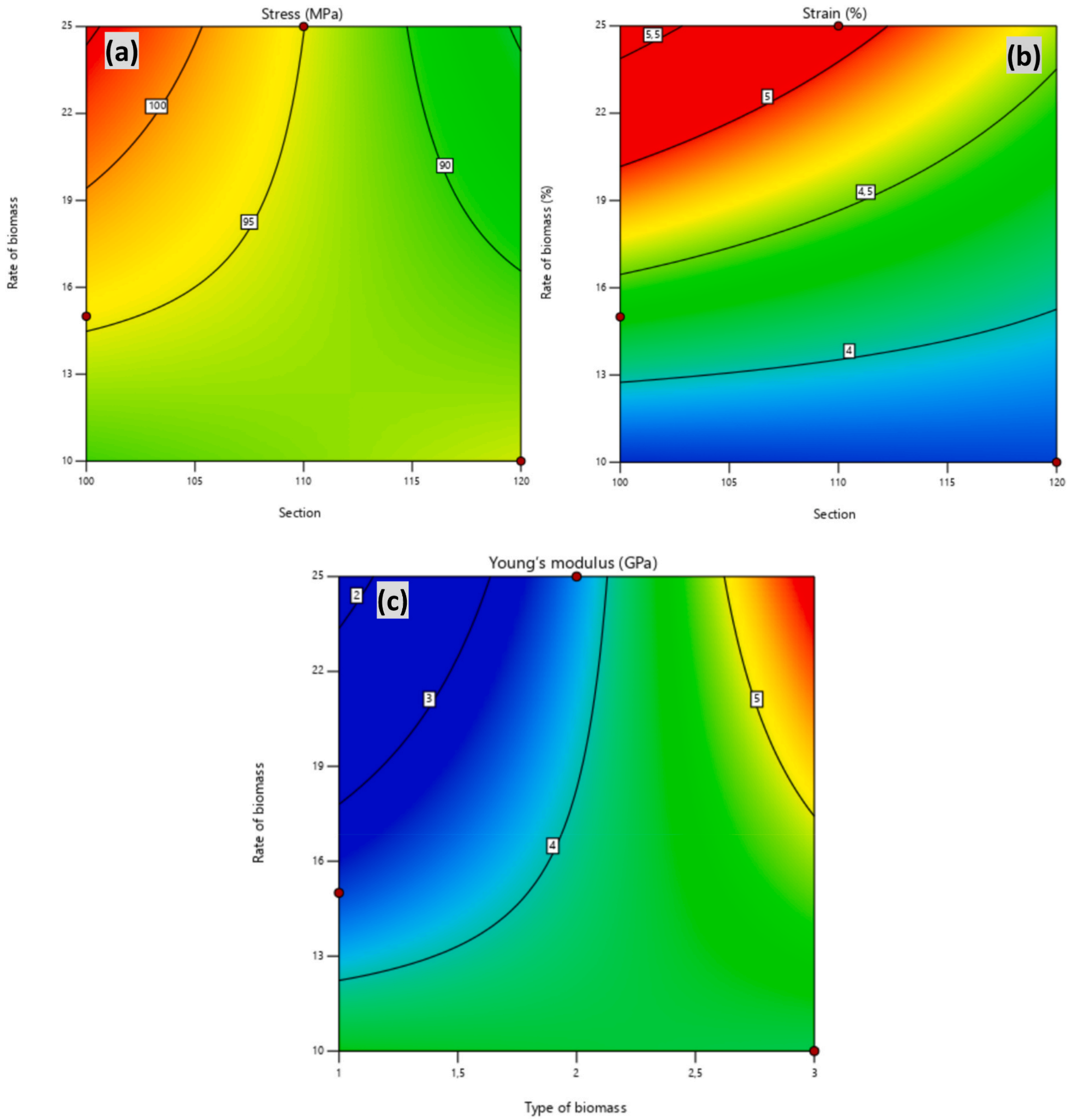

Fig. 13. Two-dimensional response surface contour plots evaluating the interactive effects of operational variables on the mechanical properties of biocomposites: (a) ultimate tensile strength (Stress), (b) elongation at break (Strain), and (c) Young's modulus.

that at these sections, the material can withstand greater tensile forces when biomass rate is reduced. Conversely, at lower sections and biomass rates, the tensile stress is comparatively lower, indicating a potential interaction between section position and biomass in determining material strength. Moving to Fig. 13b, the contour plot illustrates that strain generally decreases with increasing section number, with the highest strain values (around 5.5%) occurring at the lower sections and biomass rates. This pattern suggests that materials at the beginning sections and lower biomass rates tend to deform more under stress, possibly due to less material density or different microstructural characteristics. As the section number and biomass rate increase, the strain values diminish, stabilizing around 1%, which could imply a stiffer or more resistant material at higher sections or biomass levels. Fig. 13c focuses on Young's modulus, revealing that it tends to increase with the biomass type, with the highest modulus values (up to approximately 4 GPa) observed at the highest biomass types, particularly at higher sections. This trend suggests that the overall stiffness of the material improves with certain biomass types, especially when combined with higher sections, potentially due to changes in material composition or structural integrity. Collectively, these contour plots emphasize that the mechanical properties are strongly dependent on both the section position and biomass rate, with complex interactions influencing material performance [64]. Optimizing these parameters could be crucial for tailoring material properties to specific engineering or biological applications, ensuring the desired balance between strength, flexibility, and stiffness [65] (see Fig. 13).

3.4.4. Three-dimensional response surface analysis

Fig. 14 presents 3D response surface plots showing the coupled effects of biomass parameters on mechanical properties. The surfaces reveal clear interaction trends, where tensile stress increases with higher section values and lower biomass rates, strain decreases with increasing section and biomass content, and Young's modulus generally improves with higher biomass type and loading. Overall, the plots highlight strong

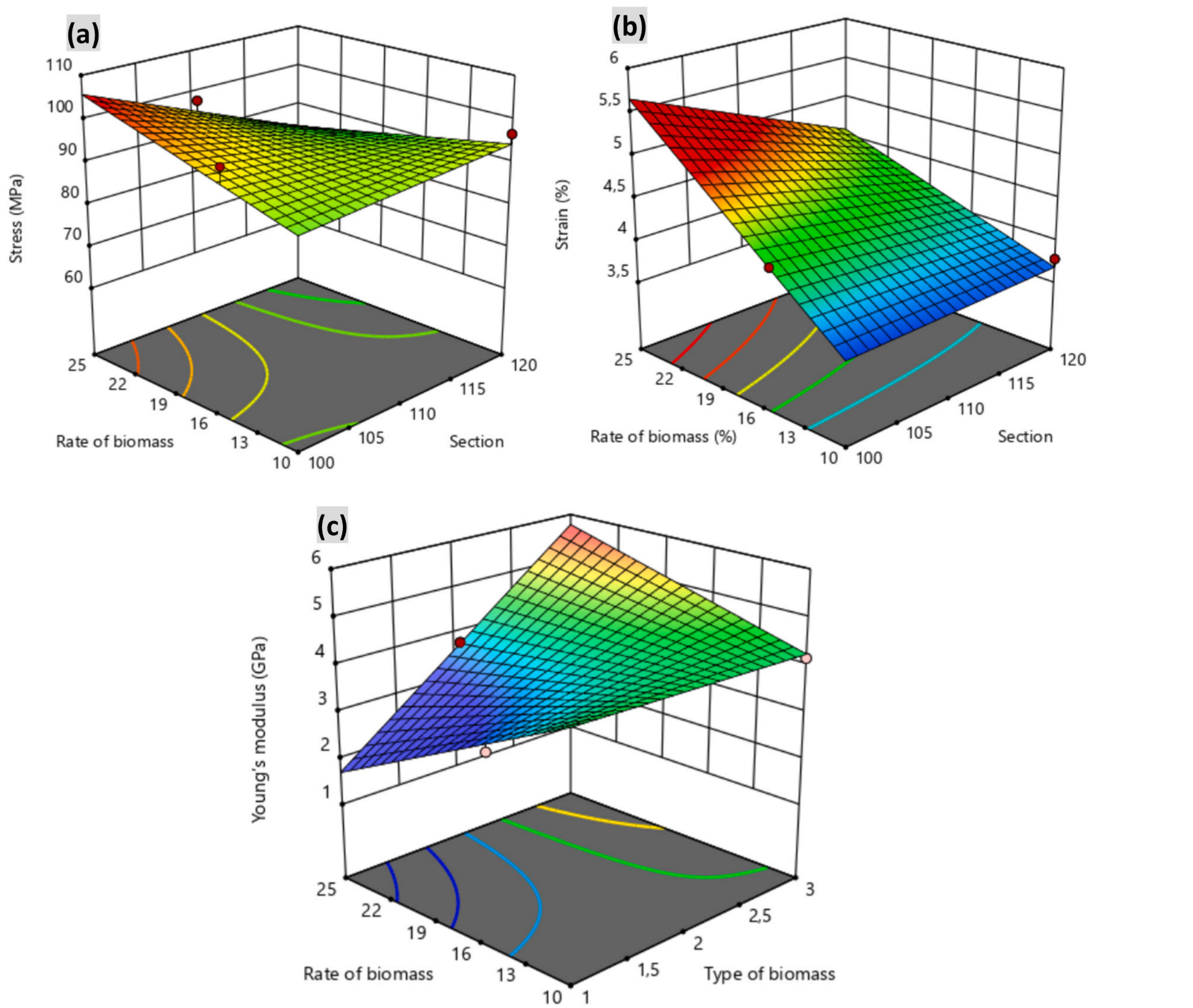

Fig. 14. Three-dimensional (3D) response surface plots modeling the interactive effects of formulation variables on the mechanical performance of biocomposites: (a) ultimate tensile strength (Stress), (b) elongation at break (Strain), and (c) Young's modulus.

nonlinear interactions between variables and provide a clear basis for optimizing composite performance.

3.4.5. Perturbation plot and factor sensitivity analysis

Fig. 15 presents perturbation plots illustrating the sensitivity of tensile stress, strain, and Young's modulus to variations in the input factors (A, B, and C) around a reference point. In plot (a), tensile stress is most strongly influenced by factor B, which shows a steep positive slope, indicating that increasing B significantly increases stress. Factor A exhibits a negative effect, as stress decreases with increasing A, while factor C has a relatively minor and nearly constant influence. In plot (b), strain is predominantly affected by factor C, which shows a strong positive trend, whereas factor A negatively influences strain and factor B has only a slight effect, indicating minimal sensitivity. In plot (c), Young's modulus is mainly governed by factors A and B, both of which display positive slopes, suggesting that increases in these factors enhance the modulus. Conversely, factor C shows a slight negative or negligible effect. Overall, the perturbation analysis reveals that different mechanical properties are controlled by different dominant factors, with B being critical for tensile stress, C for strain, and A and B jointly influencing young's modulus.

3.5. Comparison of ANN and RSM model predictions with experimental results

Fig. 16 compares the experimental results with the predictions obtained from the ANN model and the RSM regression model for (a) tensile stress, (b) strain, and (c) Young's modulus across different specimens. In all three subplots, both ANN and RSM predictions closely follow the experimental trends, indicating good agreement and reliable predictive capability. For tensile stress (a), the ANN predictions align slightly more closely with the experimental values than the RSM results, particularly at peak and low points, suggesting higher accuracy in capturing variations. In the case of strain (b), both models track the general trend, though some deviations are observed at certain specimens, with ANN again showing marginally better consistency. For Young's modulus (c), the predictions from both ANN and RSM are in strong agreement with the experimental data, with minimal discrepancies across all specimens. Overall, the figure demonstrates that while both models are effective, the ANN model achieves slightly higher prediction accuracy and better captures nonlinear variations than the RSM approach.

Table 10 presents a comparative analysis of experimental results with predictions obtained from ANN and RSM models for the mechanical properties of different biocomposites at varying weight fractions. Overall, both ANN and RSM models demonstrate good agreement with

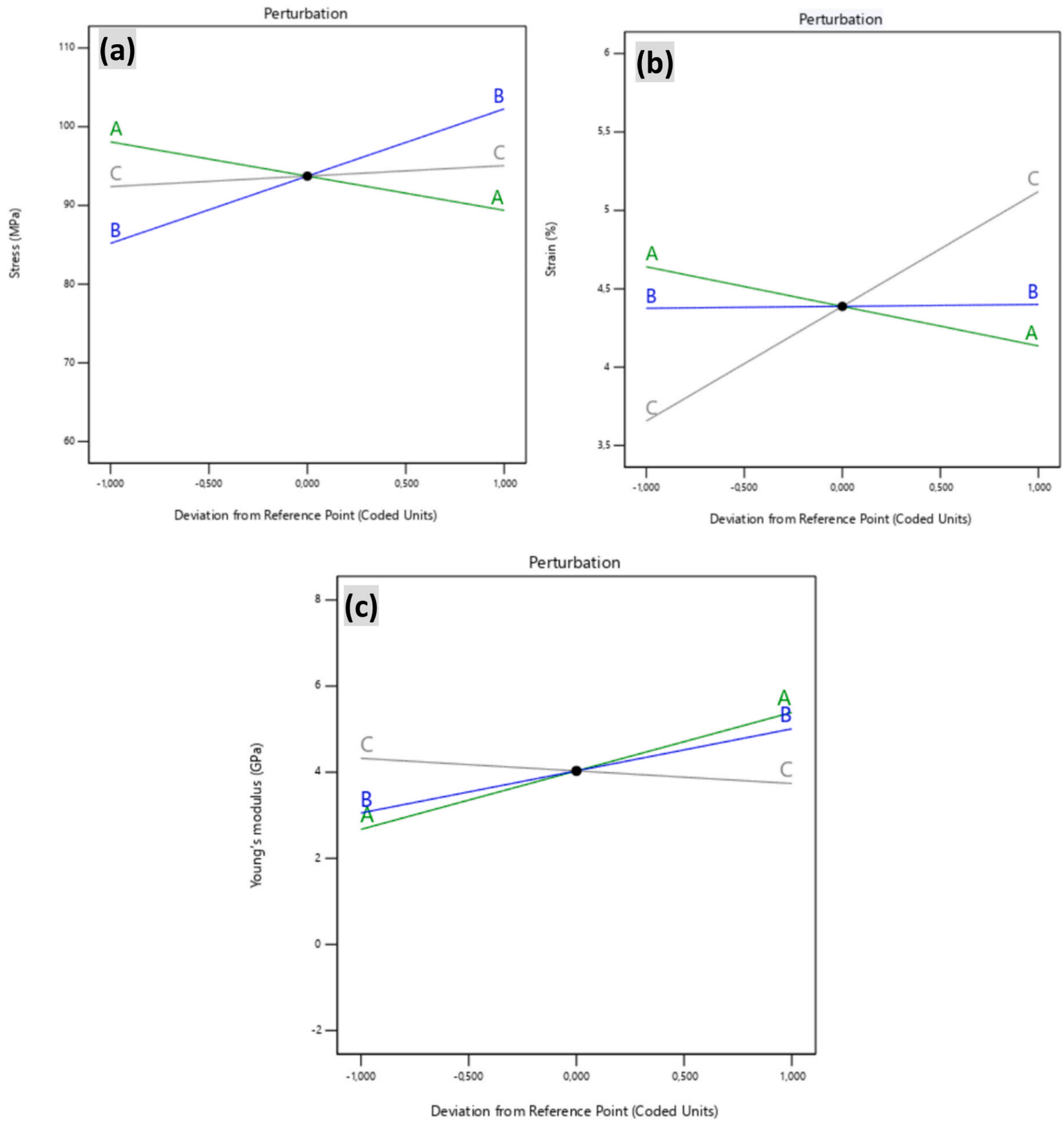

Fig. 15. Perturbation profiles evaluating response sensitivity to isolated changes in formulation and design factors around a central reference point: (a) ultimate tensile strength, (b) failure strain, and (c) Young's modulus.

the experimental data across tensile stress, strain, and young's modulus, confirming their reliability for property prediction. The ANN model generally shows closer alignment with experimental values, with smaller deviations observed in most cases, particularly for tensile stress and young's modulus. In contrast, the RSM model also follows the same trends but exhibits slightly larger variations at certain points, especially at intermediate and higher weight percentages.

For the Wb/epoxy composites, tensile stress and Young's modulus increase with increasing weight fraction, and both models successfully capture this trend, with ANN predictions being slightly more accurate. A similar pattern is observed for Ab/epoxy composites, although minor discrepancies appear in strain predictions, where ANN tends to slightly overestimate values. In the case of Pb/epoxy composites, both models effectively predict the variations in properties, including the relatively higher Young's modulus at lower weight fraction and the increase in tensile stress at higher loading.

In general, Table 10 indicates that increasing filler content tends to enhance tensile stress and stiffness (Young's modulus), while strain shows less consistent variation depending on the composite type. The close correspondence between experimental and predicted values demonstrates that both ANN and RSM models are capable of capturing the material behavior, with ANN providing marginally better predictive accuracy and consistency across different composite systems.

It is clear from analyzing the experiment results using RSM and ANN techniques that both strategies yield reliable results. Experimental verification occurs when measured parameters reach appropriate levels in order to assess the accuracy of experimental data. Mohammed Ajmal et al. [22] carried out the same study, and when compared to Mohammed, our results match and are superior using RSM and ANN.

3.6. Quantitative sustainability metrics

To go beyond the qualitative statements and make an evidence-based sustainability assessment, it was decided to conduct a preliminary

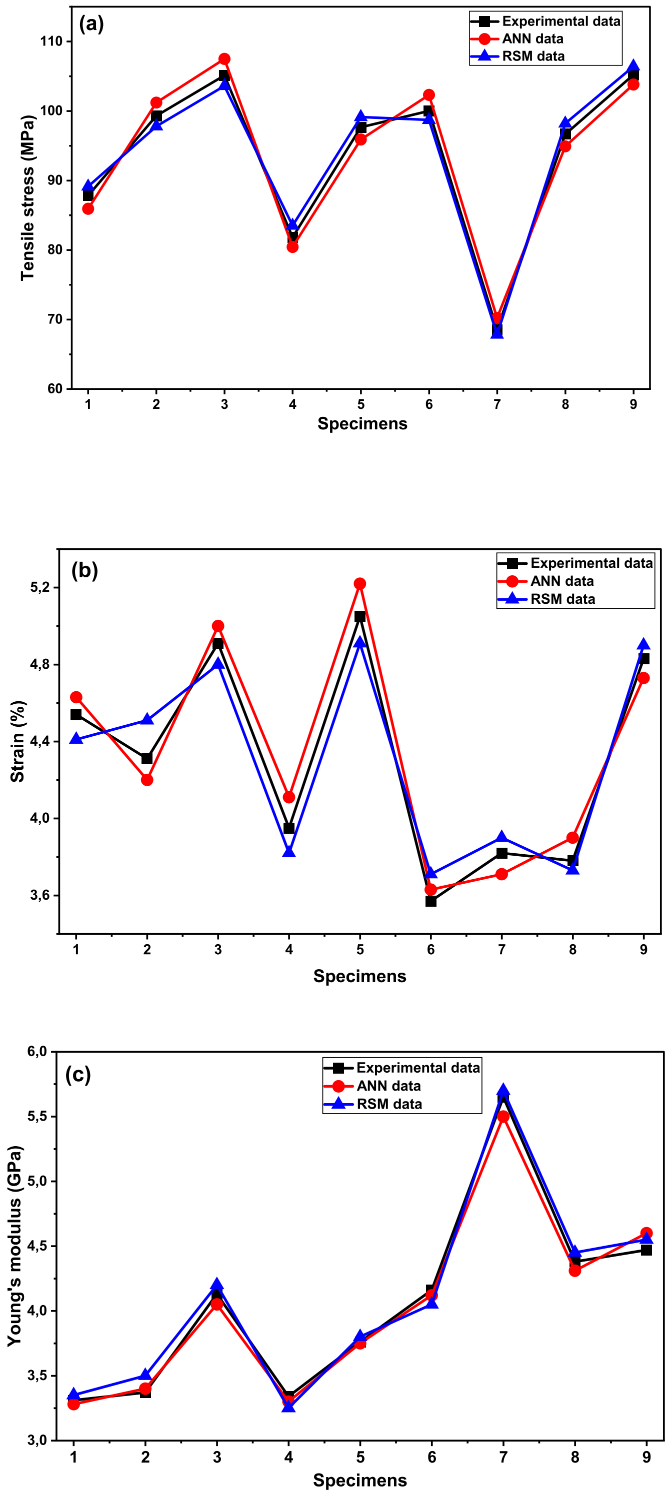

Fig. 16. Comparative line profiles validating experimental data trends against ANN and RSM model predictions across 9 distinct biocomposite formulations: (a) ultimate tensile strength, (b) failure strain, and (c) Young's modulus.

lifecycle assessment (LCA) for the best-performing composite formulation (Walnut shell/Epoxy (Wb/epoxy) 25 wt% biomass loading) against neat epoxy (0 wt% biomass). The analysis was based on a cradle-to-gate system boundary, which included raw material extraction, biomass processing (washing, drying, grinding, and sieving), and the production of epoxy resin (LY556 and HY951 hardener), along with the hand lay-up fabrication and specimen preparation for tensile testing. To make a fair comparison based on performance, the functional unit that was used was 1 kg of composite material with a tensile strength of ≥100 MPa. The inventory analysis was carried out using the Eco invent 3.8 database and the software open CA 2.0, considering background data if needed, when the contexts were adapted to the Algerian context.

The results show that the global warming potential (GWP, 100-year time frame) of the Wb/epoxy (25 wt%) composite is reduced by ~18% compared to neat epoxy (3.21 kg CO_2 eq for kg of material vs. 3.92 kg CO_2 eq for kg of material). This reduction is mostly due to two reasons: (1) replacing the petroleum-based epoxy resin with renewable and agricultural waste-derived walnut shell particles and (2) the sequestration of CO_2 during the growth phase of walnut trees in the biomass filler. Also, the cumulative energy demand (CED) for the biocomposite is 14% (78.5 MJ/kg biocomposite versus 91.3 MJ/kg of neat epoxy) lower than that of neat epoxy, which suggests that the biocomposite is less dependent on fossil fuels.

But a number of constraints need to be recognized in relation to environmental durability and end-of-life routes. Because of the thermosetting property of epoxy matrix, the biocomposite can't be remelted and can't be directly recycled into new high-performance composites using conventional technologies. However, it remains a viable route of recycling for discarded composites to be ground up into fine particles to be used in low-load bearing applications (such as construction panels and non-structural infills) and is called downcycling. Chemical recycling processes (such as solvolysis for the depolymerization of epoxy) are still at laboratory level and are not yet commercially ready. As far as environmental durability is concerned, accelerated hygrothermal aging tests (70 °C, 85%RH, 500 h) on the Wb/epoxy (25 wt%) composite showed that the composite's tensile strength decreased by 12% and the water absorption increased by 9% from that of neat epoxy, suggesting that the composite performed well under ambient conditions, although moisture ingress in the interface between matrix and filler is a concern for outdoor structural applications that are not protected by either surface treatment or coating.

These quantitative metrics provide a quantitative confirmation of the measurable environmental advantage that walnut shell/epoxy composites can provide over neat epoxy, in addition to revealing the need for further research into how to create environmentally durable applications and recycling strategies at the end of the composites' useful life. This evidence-based assessment makes the sustainability conversation from conceptual to quantitative, echoing the environmental claims of this study.

4. Conclusion

The tensile performance of epoxy composites filled with three agricultural biomass materials – walnut shells (Wb), almond shells (Ab), and pistachio shells (Pb) – at the weight percentage of 10, 15 and 25, with the cross section of 100, 110 and 120 mm^2 were studied comprehensively. Experimental results clearly show that the choice of the filler type and amount significantly affects the mechanical properties. Walnut shell-reinforced composites (Wb/epoxy) demonstrated highest tensile strength values (up to 105.12 MPa at 25 wt%) and ductility (strain ~4.9%) which were related to uniform dispersion of the particles, strong interactions between the particle and matrix and minimum microstructural defects as confirmed by SEM analysis among three fillers studied. Almond shell and pistachio shell composites, on the other hand, exhibited lower strains for higher loadings (such as ~3.6% at 25 wt% of Ab) because the particles were prone to agglomeration, formation of microvoids, and local debonding that increased the concentration of stresses and reduced the efficiency of the load transfer.

ANN and RSM were used to estimate tensile stress, tensile strain, and Young's Modulus from a predictive modeling point of view – both models were useful with ANN providing slightly greater accuracy to capture the nonlinear trends. However, the validation of ANN was limited by the limited dataset, which indicates the need for larger and

Table 10
Comparison of experimental/ANN/RSM of the mechanical properties for biocomposites.

Composite	N°	Wt (%)	Experimental data			ANN data			RSM data		
			Stress (MPa)	Strain (%)	Young's modulus (GPa)	Stress (MPa)	Strain (%)	Young's modulus (GPa)	Stress (MPa)	Strain (%)	Young's modulus (GPa)
Wb/ epoxy	1	10	87.82	4.54	3.31	85.92	4.63	3.28	89.13	4.41	3.35
	2	15	99.31	4.31	3.37	101.21	4.20	3.40	97.80	4.51	3.50
	3	25	105.12	4.91	4.13	107.50	5.00	4.05	103.61	4.80	4.20
Ab/epoxy	4	10	81.82	3.95	3.34	80.43	4.11	3.30	83.50	3.82	3.25
	5	15	97.66	5.05	3.76	95.89	5.22	3.75	99.13	4.91	3.80
	6	25	100.01	3.57	4.16	102.31	3.63	4.12	98.71	3.71	4.05
Pb/epoxy	7	10	68.54	3.82	5.65	70.19	3.71	5.50	67.80	3.90	5.70
	8	15	96.66	3.78	4.38	94.90	3.90	4.31	98.20	3.73	4.45
	9	25	105.2	4.83	4.47	103.81	4.73	4.60	106.42	4.90	4.55

more balanced experimental datasets for robust generalization. The appearance of NaN correlation coefficients in the sets of the validation sets is also a sign of this. Although less accurate, RSM gave some statistical information about the interactions between the factors, showing that the biomass type dominates the tensile stress; the strain dominates the biomass weight fraction; and the biomass type and cross section area together dominate the Young's modulus.

Importantly, this study has some limitations. First, the filler weight fraction was limited to 25 wt% max which needs to be further validated by experiments beyond this value. Second, the hand lay-up fabrication technique which is practical can introduce variation in dispersion of particles. Third, the predictive models have been tested for only a limited range of mechanical properties and not for other ones like flexural, impact or fatigue properties.

Based on these results, the following points are recommended for future research: (1) to study the hybrid biomass filler system or the use of nano-sized reinforcement to increase strength and toughness; (2) to consider the use of advanced surface treatments such as silane coupling agents to improve the bonding between the reinforcement and the polymer, and to minimize agglomeration effect with the increase of reinforcement quantity; (3) to apply the advanced modeling technology based on artificial intelligence to predict thermal, hygrothermal, and long-term aging properties; and (4) to carry out lifecycle assessment and cost-benefit analysis to support industrial scalability. Further, it will be recognized that extrapolation to more than 25 wt% is not fully validated by experiments.

Overall, this study develops a robust, AI-driven design process for the development of sustainable, high-performance epoxy biocomposites using agricultural waste, which could provide a promising route towards eco-friendly structural materials without sacrificing their mechanical properties.

Declaration of competing interest

The authors declare that they have no known competing financial interests or personal relationships that could have appeared to influence the work reported in this paper.

Acknowledgements

No funding.

References

[1] Lamia B, Nafissa M, Abdelouahab Djoubair B, Jawaid M, Fouad H, Midani M. New cellulosic fibre from spathes of male date for lightweight composite materials: extraction and characterization. J Mater Res Technol 2023;24:5361–71. https://doi.org/10.1016/j.jmrt.2023.04.159.

[2] Singh VK. Identification of the tensile properties of hybrid composite material by artificial neural network. 2014. https://asjp.cerist.dz/en/article/2369.

[3] Elfaleh I, Abbassi F, Habibi M, Ahmad F, Guedri M, Nasri M, Garnier C. A comprehensive review of natural fibers and their composites: an eco-friendly alternative to conventional materials. Results Eng 2023;19:101271. https://doi.org/10.1016/j.rineng.2023.101271.

[4] Kangishwar S, Radhika N, Sheik AA, Chavali A, Hariharan S. A comprehensive review on polymer matrix composites: material selection, fabrication, and application. Polym Bull 2023;80:47–87. https://doi.org/10.1007/s00289-022-04087-4.

[5] Rajak DK, Pagar DD, Menezes PL, Linul E. Fiber-reinforced polymer composites: manufacturing, properties, and applications. Polymers 2019;11:1667. https://doi.org/10.3390/polym11101667.

[6] Freitas BR, Braga JO, Orlandi MP, da Silva BP, Aoki IV, Lins VFC, Cotting F. Characterization of coir fiber powder (Cocos nucifera L.) as an environmentally friendly inhibitor pigment for organic coatings. J Mater Res Technol 2022;19:1332–42. https://doi.org/10.1016/j.jmrt.2022.05.098.

[7] Lau K, Hung P, Zhu M-H, Hui D. Properties of natural fibre composites for structural engineering applications. Composites, Part B Eng 2018;136:222–33. https://doi.org/10.1016/j.compositesb.2017.10.038.

[8] Pulikkalparambil H, Varghese SA, Chonhenchob V, Nampitch T, Jarupan L, Harnkarnsujarit N. Recent advances in natural fibre-based materials for food packaging applications. Polymers 2023;15:1393. https://doi.org/10.3390/polym15061393.

[9] Ali HT, Alghtani AH, Felemban BF, Abd El-Aziz K, Saber D, Ahmed EM, Megahed M, Fotouhi M. Multivariable analysis for selection of natural fibers as fillers for a sustainable food packaging industry. Mater Res Express 2021;8:95504. https://doi.org/10.1088/2053-1591/ac17a9.

[10] Naik V, Kumar M, Vijayan V, Kaup A. A review on natural fiber composite material in automotive applications. Eng Sci 2022;18:1–10. https://doi.org/10.30919/es8d589.

[11] Huda MS, Drzal LT, Ray D, Mohanty AK, Mishra M. 7 - natural-fiber composites in the automotive sector. In: Pickering, editor. Woodhead publ. Ser. Compos. Sci. Eng. Woodhead Publishing; 2008. p. 221–68. https://doi.org/10.1533/9781845694593.2.221. K.L.B.T.-P. and P. of N.-F.C.

[12] Mohankumararadhya HM, Wadappi P, Chandrashekar A, Naik Y. Studies on bio waste product particle reinforced polymer composites. In: AIP conf. Proc., 2274; 2020. https://doi.org/10.1063/5.0022746.

[13] Mohankumararadhya HM, Wadappi P, Chandrashekar A, Naik Y. Studies on bio waste product particle reinforced polymer composites. In: AIP Conf. Proc. AIP Publishing LLC; 2020, 30047. https://doi.org/10.1063/5.0022746.

[14] Olumuyiwa AJ, Isaac TS, Samuel SO. Study of mechanical behaviour of coconut shell reinforced polymer matrix composite. J Miner Mater Char Eng 2012;11:774–9. https://www.researchgate.net/profile/S-Talabi/publication/256369643_Study_of_Mechanical_Behaviour_of_Coconut_Shell_Reinforced_Polymer_Matrix_Composite/links/004635225e2302a5b7000000/Study-of-Mechanical-Behaviour-of-Coconut-Shell-Reinforced-Polymer-Matrix-.

[15] Shettar M, Bhat A, Katagi NN, Gowrishankar MC. Experimental investigation on mechanical properties of glass fiber–nanoclay–epoxy composites under water-soaking: a comparative study using RSM and ANN. J Compos Sci 2025;9. https://doi.org/10.3390/jcs9040195.

[16] Antil SK, Antil P, Singh S, Kumar A, Pruncu CI. Artificial neural network and response surface methodology based analysis on solid particle erosion behavior of polymer matrix composites. Materials 2020;13:1381. https://doi.org/10.3390/ma13061381.

[17] Arunachalam SJ, Saravanan R, Sathish T, Giri J, Kanan M. Mechanical assessment for enhancing hybrid composite performance through silane treatment using RSM and ANN. Results Eng 2024;24:103309. https://doi.org/10.1016/j.rineng.2024.103309.

[18] Vinoth V, Sathiyamurthy S, Saravanakumar S, Senthilkumar R. Integrating response surface methodology and machine learning for analyzing the unconventional machining properties of hybrid fiber-reinforced composites. Polym Compos 2024;45:6077–92. https://doi.org/10.1002/pc.28180.

[19] Kopparthi PK, Kundavarapu VR, Dasari VR, Kaki VR, Pathakokila BR. Modeling of glass fiber reinforced composites for optimal mechanical properties using teaching learning based optimization and artificial neural networks. SN Appl Sci 2019;2:131. https://doi.org/10.1007/s42452-019-1837-x.

[20] Arunachalam SJ, Saravanan R, Othman NA, Thanikodi S, Giri J, Azizi M, Saidani T. Artificial intelligence-driven prediction and optimization of tensile and impact strength in natural fiber/aluminum oxide polymer nanocomposites. Eng Rep 2025;7:1–20. https://doi.org/10.1002/eng2.70093.

[21] Heitkamp T, Hilbig K, Goutier M, Girnth S, Waldt N, Klawitter G, Vietor T. Characterization of mechanical properties , efficiency , and design considerations for the additive manufacturing of hybrid composites with continuous fibers. Hybrid Adv 2024;5:100146. https://doi.org/10.1016/j.hybadv.2024.100146.
[22] Mohammed Ajmal SF, Natrayan L, Giri J, Makki E, Shah MA, Mallik S. Utilization of response surface methodology to optimize the mechanical behaviour of flax/nano TiO2/Epoxy based hybrid composites under liquid nitrogen environment. Front Mater 2024;11:1344351. https://doi.org/10.3389/fmats.2024.1344351.
[23] Sari NH, Wardana ING, Irawan YS, Siswanto E. Physical and acoustical properties of corn husk fiber panels. Adv Acoust Vib 2016;2016:5971814. https://doi.org/10.1155/2016/5971814.
[24] Saravanan KA, Arunachalam N, Uma P, Saravanan K, Arunachalam J. Modelling for predicting and optimizing of the tensile and flexural properties of Sisal/carbon fibre nanocomposite through RSM. J Environ Nanotechnol 2024;13:467–77.
[25] Natarajan P, Mohanraj M, Kumar M, Sathish S. Experimental investigation on mechanical and tribological analysis of pineapple leaf (Ananas comosus) and sisal (Agave sisalana) fibers reinforced hybrid epoxy composites. Int Polym Process 2024;39:134–42. https://doi.org/10.1515/ipp-2023-4433.
[26] Mathad S. Investigation of mechanical properties of sisal fiber reinforced polymer investigation of mechanical properties of sisal fiber reinforced polymer composites. 2017. https://doi.org/10.21467/ajgr.1.1.40-48.
[27] Ofuyatan OM, Agbawhe OB, Omole DO, Igwegbe CA, Ighalo JO. RSM and ANN modelling of the mechanical properties of self-compacting concrete with silica fume and plastic waste as partial constituent replacement. Clean Mater 2022;4:100065. https://doi.org/10.1016/j.clema.2022.100065.
[28] Nikoo M, Hafeez G. Period estimate of wood buildings employing soft modelling techniques. Soft Comput 2023;27:16251–64. https://doi.org/10.1007/s00500-023-08040-z.
[29] Kurt Z, Yilmaz Y, Cakmak T, Ustabaş I. A novel framework for strength prediction of geopolymer mortar: renovative precursor effect. J Build Eng 2023;76:107041. https://doi.org/10.1016/j.jobe.2023.107041.
[30] Dhanalakshmi A, Shahul Hameed M, Valarmathi K, Rajendra Prasath C. Investigation on compressive strength of fibre-reinforced concrete using artificial neural network. Lect Notes Civ Eng 2024;459:13–24. https://doi.org/10.1007/978-981-97-0072-1_2.
[31] Nikoo M, Hadzima-Nyarko M, Karlo Nyarko E, Nikoo M. Determining the natural frequency of cantilever beams using ANN and heuristic search. Appl Artif Intell 2018;32:309–34. https://doi.org/10.1080/08839514.2018.1448003.
[32] dua S, Khatri H, Naveen J, Jawaid M, Jayakrishna K, Norrrahim MNF, Rashedi A. Potential of natural fiber based polymeric composites for cleaner automotive component production -a comprehensive review. J Mater Res Technol 2023;25:1086–104. https://doi.org/10.1016/j.jmrt.2023.06.019.
[33] Benyettou R, Amroune S, Slamani M, Saada K, Fouad H, Jawaid M, Sikdar S. Modelling and optimization of the absorption rate of date palm fiber reinforced composite using response surface methodology. Alex Eng J 2023;79:545–55. https://doi.org/10.1016/j.aej.2023.08.042.
[34] Saada K, Amroune S, Zaoui M, Jawaid M, Benarioua M, Farsi C. Optimizing water Absorption's influence on composite mechanics through response surface methodology. J Compos Mater 2024;58:2327–41. https://doi.org/10.1177/00219983241264357.
[35] Ghadai RK, Kalita K, Mondal SC, Swain BP. PECVD process parameter optimization: towards increased hardness of diamond-like carbon thin films. Mater Manuf Process 2018;33:1905–13. https://doi.org/10.1080/10426914.2018.1512114.
[36] Kalita K, Dey P, Haldar S. Search for accurate RSM metamodels for structural engineering. J Reinforc Plast Compos 2019;38:995–1013. https://doi.org/10.1177/0731684419862346.
[37] Papajová I, Juriš P, Szabová E, Venglovský J, Sasáková N, Šefčíková H, Martinez J, Gáboň T. Decontamination by anaerobic stabilisation of the environment contaminated with enteronematode eggs Toxocara canis and Ascaris suum. Bioresour Technol 2008;99:4966–71. https://doi.org/10.1016/j.biortech.2007.09.044.
[38] Faruk O, Bledzki AK, Fink H-P, Sain M. Biocomposites reinforced with natural fibers: 2000–2010. Prog Polym Sci 2012;37:1552–96. https://doi.org/10.1016/j.progpolymsci.2012.04.003.
[39] Jawaid M, Abdul Khalil HPS. Cellulosic/synthetic fibre reinforced polymer hybrid composites: a review. Carbohydr Polym 2011;86:1–18. https://doi.org/10.1016/j.carbpol.2011.04.043.
[40] Pickering KL, Efendy MGA, Le TM. A review of recent developments in natural fibre composites and their mechanical performance. Compos Part A Appl Sci Manuf 2016;83:98–112. https://doi.org/10.1016/j.compositesa.2015.08.038.
[41] Dhakal HN, Zhang ZY, Richardson MOW. Effect of water absorption on the mechanical properties of hemp fibre reinforced unsaturated polyester composites. Compos Sci Technol 2007;67:1674–83. https://doi.org/10.1016/j.compscitech.2006.06.019.
[42] Pickering K. Properties and performance of natural-fibre composites. Elsevier; 2008. https://doi.org/10.1533/9781845694593.
[43] Behera K, Chen J-F, Yang J-M, Chang Y-H, Chiu F-C. Evident improvement in burning anti-dripping performance, ductility and electrical conductivity of PLA/PVDF/PMMA ternary blend-based nanocomposites with additions of carbon nanotubes and organoclay. Composites, Part B Eng 2023;248:110371. https://doi.org/10.1016/j.compositesb.2022.110371.
[44] Ghani MU, Sun B, Houda M, Zeng S, Khan MB, ElDin HMS, Waqar A, Benjeddou O. Mechanical and environmental evaluation of PET plastic-graphene nano platelets concrete mixes for sustainable construction. Results Eng 2024;21:101825. https://doi.org/10.1016/j.rineng.2024.101825.
[45] Kumar KS, Srinivasan RG, Palani S, Čep R, Salunkhe S, Nasr EA. Mechanical characterization of sisal fiber-groundnut shell powder reinforced epoxy composites. Sci Rep 2025;15:33149. https://doi.org/10.1038/s41598-025-18645-z.
[46] Sklyar VG, Firer VI. Investigation of mechanical properties of electrodeposited gold. Ind Lab 1983;49:205–8. https://doi.org/10.13140/RG.2.2.18932.58244.
[47] Al Mamun MA, Aftab H, Hasan MH, Khan MA, Rahman GMS. From agricultural waste to eco-composites: peanut shell powder in jute-fabric-reinforced unsaturated polyester resin. ChemistrySelect 2025;10:e02119. https://doi.org/10.1002/slct.202502119.
[48] Sanjay MR, Madhu P, Jawaid M, Senthamaraikannan P, Senthil S, Pradeep S. Characterization and properties of natural fiber polymer composites: a comprehensive review. J Clean Prod 2018;172. https://doi.org/10.1016/j.jclepro.2017.10.101.
[49] Singh AAMM, Franco PA, Azhagesan N, Sharun V. Exploring seashell and rice husk waste for lightweight hybrid biocomposites: synthesis, microstructure, and mechanical performance. Biomass Convers Biorefinery 2023. https://doi.org/10.1007/s13399-023-04846-x.
[50] Li X, Ho CM, Doh SI, Al Biajawi MI, Ma Q, Zhao D, Liu R. Strength characteristics and prediction of ternary blended cement building material using RSM and ANN. Buildings 2025;15:733. https://doi.org/10.3390/buildings15050733.
[51] Aydoğmuş E, Arslanoğlu H, Dağ M. Production of waste polyethylene terephthalate reinforced biocomposite with RSM design and evaluation of thermophysical properties by ANN. J Build Eng 2021;44:103337. https://doi.org/10.1016/j.jobe.2021.103337.
[52] Armaghani DJ, Asteris PG. A comparative study of ANN and ANFIS models for the prediction of cement-based mortar materials compressive strength. Neural Comput Appl 2021;33:4501–32. https://doi.org/10.1007/s00521-020-05244-4.
[53] Kooshkaki A, Eskandari-Naddaf H. Effect of porosity on predicting compressive and flexural strength of cement mortar containing micro and nano-silica by multi-objective ANN modeling. Constr Build Mater 2019;212:176–91. https://doi.org/10.1016/j.conbuildmat.2019.03.243.
[54] Eskandari-Naddaf H, Kazemi R. ANN prediction of cement mortar compressive strength, influence of cement strength class. Constr Build Mater 2017;138:1–11. https://doi.org/10.1016/j.conbuildmat.2017.01.132.
[55] Nasri K, Toubal L. Artificial neural network approach for assessing mechanical properties and impact performance of natural-fiber composites exposed to UV radiation. Polymers 2024;16:538. https://doi.org/10.3390/polym16040538.
[56] Brito Oliveira GA, Freire Júnior RCS, Barbosa JF, Correia JAFO. An approach to predict ultimate transverse tensile strength based on mixed ANN models for a composite lamina. J Mater Res Technol 2023;23:2719–29. https://doi.org/10.1016/j.jmrt.2023.01.195.
[57] Singh K, Adhikari J, Roscow J. Prediction of the electromechanical properties of a piezoelectric composite material through the artificial neural network. Mater Today Commun 2024;38:108288. https://doi.org/10.1016/j.mtcomm.2024.108288.
[58] Aghabalaei Baghaei K, Hadigheh SA. Artificial neural network prediction of transverse modulus in humid conditions for randomly distributed unidirectional fibre reinforced composites: a micromechanics approach. Compos Struct 2024;337:118073. https://doi.org/10.1016/j.compstruct.2024.118073.
[59] Bai J-B, Bu G-Y, Wang ZZ, Cao P-C, Li X-Q, Guo S-X, Liu T-W. Rapid prediction of mechanical properties during composite curing using artificial neural network and multi-objective genetic algorithms. Compos Struct 2025;354:118809. https://doi.org/10.1016/j.compstruct.2024.118809.
[60] Arunachalam SJ, Saravanan R, Sathish T, Alarfaj AA, Giri J, Kumar A. Enhancing mechanical performance of MWCNT filler with jute/kenaf/glass composite: a statistical optimization study using RSM and ANN. Mater Technol 2024;39:1–15. https://doi.org/10.1080/10667857.2024.2381156.
[61] Marrubini G, Dugheri S, Cappelli G, Arcangeli G, Mucci N, Appelblad P, Melzi C, Speltini A. Experimental designs for solid-phase microextraction method development in bioanalysis: a review. Anal Chim Acta 2020;1119:77–100. https://doi.org/10.1016/j.aca.2020.04.012.
[62] Morshed MN, Pervez MN, Behary N, Bouazizi N, Guan J, Nierstrasz VA. Statistical modeling and optimization of heterogeneous Fenton-like removal of organic pollutant using fibrous catalysts: a full factorial design. Sci Rep 2020;10:16133. https://doi.org/10.1038/s41598-020-72401-z.
[63] Nor AFM, Hassan MZ, Rasid ZA, Aziz SA, Sarip S, Md Daud MY. Optimization on tensile properties of Kenaf/multi-walled CNT hybrid composites with box-behnken design. Appl Compos Mater 2021;28:607–32. https://doi.org/10.1007/s10443-021-09879-x.
[64] Saravanan KA, Arunachalam N, Uma P, Saravanan K, Arunachalam J. Modelling for predicting and optimizing of the tensile and flexural properties of sisal/carbon fibre nano-composite through RSM. J Environ Nanotechnol 2024;13:467–77. https://doi.org/10.13074/jent.2024.09.242674.
[65] Nugroho G, Budiyantoro C. Optimization of fiber factors on flexural properties for carbon fiber reinforced polypropylene. J Compos Sci 2022;6:160. https://doi.org/10.3390/jcs6060160.